END

DATE
FILMED

5-81

DTIC

1.0

2.8   2.5

3.2

3.6   2.2

2.0

1.1

1.8

1.25   1.4   1.6

MICROCOPY RESOLUTION TEST CHART

Application of Ion Implantation for the Improvement of Localized Corrosion Resistance of M50 Steel Bearings

G. K. Hubler, J. K. Hirvonen, and C. R. Gossett

Materials Modification & Analysis Branch
Condensed Matter & Radiation Sciences Division

I. Singer

Surface Chemistry Branch
Chemistry Division

C. R. Clayton and Y. F. Wang

State University of New York
Stony Brook, NY 11794

H. E. Munson

TRW Bearings Division
402 Chandler Street
Jamestown, NY 14701

AND

G. Kuhlman

Naval Air Rework Facility
North Island, CA

March 30, 1981

9 Memorandum rept,

REPORT DOCUMENTATION PAGE		READ INSTRUCTIONS BEFORE COMPLETING FORM
1. REPORT NUMBER (14) NRL-MR- NRL Memorandum Report 4481	2. GOVT ACCESSION NO. AD--AC97 230	3. RECIPIENT'S CATALOG NUMBER
4. TITLE (and Subtitle) (6) APPLICATION OF ION IMPLANTATION FOR THE IMPROVEMENT OF LOCALIZED CORROSION RESISTANCE OF M50 STEEL BEARINGS		5. TYPE OF REPORT & PERIOD COVERED Interim report on a continuing NRL problem.
		6. PERFORMING ORG. REPORT NUMBER
7. AUTHOR(s) (10) G. K. Hubler, J. K. Hirvonen, I. Singer, C. R. Gossett, C. R. Clayton*, Y. F. Wang*, H. E. Munson†, and G. Kuhlman**		8. CONTRACT OR GRANT NUMBER(s)
9. PERFORMING ORGANIZATION NAME AND ADDRESS Naval Research Laboratory Washington, DC 20375 (11) 30 Mar 81		10. PROGRAM ELEMENT, PROJECT, TASK AREA & WORK UNIT NUMBERS 62241N; RR-022-08-44; 66-0424-0-1
11. CONTROLLING OFFICE NAME AND ADDRESS Naval Air Propulsion Center P.O. Box 7176 (12) 48 Trenton, NJ 08628		12. REPORT DATE March 30, 1981
		13. NUMBER OF PAGES 47
14. MONITORING AGENCY NAME & ADDRESS(If different from Controlling Office) (16) RR022 08, F41401		15. SECURITY CLASS. (of this report) UNCLASSIFIED
		15a. DECLASSIFICATION/DOWNGRADING SCHEDULE

16. DISTRIBUTION STATEMENT (of this Report)

Approved for public release; distribution unlimited.

(17) RR02-0844, WF41401 00

17. DISTRIBUTION STATEMENT (of the abstract entered in Block 20, if different from Report)

18. SUPPLEMENTARY NOTES

*Present address: State University of New York, Stony Brook, NY 11794
†Present address: TRW Bearings Division, 402 Chandler Street, Jamestown, NY 14701
**Present address: Naval Air Rework Facility, North Island, CA

19. KEY WORDS (Continue on reverse side if necessary and identify by block number)

Ion implantation	M50 Bearing steel
Corrosion	
Bearings	
Surface alloys	
Bearing performance	

20. ABSTRACT (Continue on reverse side if necessary and identify by block number)

A program is currently underway to use ion implantation to improve the tribological and corrosion characteristics of load bearing surfaces in both rolling element bearings and gears used in aircraft propulsion systems.

This report describes that aspect of the program concerned with the use of ion implantation for surface alloying of bearing components in order to alleviate the problem of corrosion in M50 steel mainshaft aircraft engine bearings.

DD FORM 1473 EDITION OF 1 NOV 65 IS OBSOLETE
1 JAN 73
S/N 0102-014-6601

CONTENTS

APPLICATION OF ION IMPLANTATION FOR THE IMPROVEMENT
OF LOCALIZED CORROSION RESISTANCE OF M50 STEEL BEARINGS

I. Introduction

The high cost of replacement mainshaft bearings in turbojet engines of Navy aircraft has stimulated the need to develop longer lifetime bearings. A major cause of bearing rejection is pitting corrosion arising when chlorides and water accumulate in the engine lubricants of aircraft in intermittent use. The corrosion pits may act as initiation sites for fatigue spalling which can lead to catastrophic engine failure. Another serious field problem is that replacement bearings have a short shelf life and must be reworked every 90 days, such that a majority of the bearings reconditioned at Naval Air Rework Facilities (NARF's) are recycled bearings from the shelf, not bearings to be reworked from used aircraft engines.[1]

In response to these problems, a research program has been established at the Naval Research Laboratory for the purpose of investigating the use of ion implantation for producing corrosion resistant alloys on M-50 bearing surfaces. This work is under the support and direction of the Naval Air Propulsion Center, Trenton, NJ. NAPC is also responsible for overall planning and coordination of those aspects of the program concerned with mechanical bench testing and field evaluation of implanted components to insure that rolling contact fatigue life and bearing performance have not deteriorated.

Initial work at NRL showed that ion implantation of Cr into M50 bearing steel dramatically improved its corrosion resistance in Cl contaminated engine oil, and that implantation did not degrade the rolling contact fatigue lifetime of the material as has been found for some coatings.[2,3] Moreover, implantation produces no macroscopic dimensional changes (< 1 microinch) and is applicable to otherwise finished bearings.[4]

This report describes the progress of a two part program designed (i) to determine optimum implantation parameters for improving corrosion resistance of M50 bearing alloy steel and, (ii) to develop the technology for implanting actual bearings so that ion-implanted bearings can be engine tested for the purpose of flight evaluation. The four following sections describe in turn, progress in laboratory corrosion testing of ion implanted M50, progress in bearing implantation, progress in mechanical testing of implanted bearings, and concluding remarks. The work performed by NAPC and NRL was authorized by NAVAIR AIRTASK No. A03V3300/0528/0F4140100.

II. Laboratory Corrosion Experiments

Several types of corrosion tests were necessary to ascertain if changes in corrosion resistance occured as a result of ion implantation. To conduct these tests in actual bearings would have been expensive and time consuming. Therefore, small samples were prepared from 3/8" diameter M50 rods so that accelerated tests could be

conducted on surfaces of about 1 cm^2 in area. Flats (1/8" to 1/4" tall) were cut from the rod by means of a water cooled SiC cut-off wheel and polished to a mirror finish with diamond paste (1 μm). Alumina polishing was initially used but was replaced with the diamond polish because numerous alumina inclusions remained in the polished surfaces.

Two types of tests were performed. The first were qualitative field service simulation tests. Those ions which looked promising in simulation tests were further studied by electrochemical polarization tests which give more quantitative information. Section II describes the results of these tests on ion-implanted samples.

Since September 1978 more than 120 M50 samples (listed in Appendix) have been implanted for use either in the simulation tests or in the electrochemical tests. The ion energies have ranged between 12.5 and 150 keV, with fluences between 1 x 10^{16}/cm^2 and 4 x 10^{17}/cm^2 for the species Al, Ti, Cr, Mo, Cr+Mo, Cr+Mo+N, Cr+P, and Cr+B. The choice of implanted ions was determined by the well known corrosion behavior of the ions in bulk materials, i.e., (i) Chromium produces stainless steel when added to iron based alloys in concentrations greater than 12%,[5] (ii) Mo is known to improve pitting resistance in steels,[6] (iii) Ti and Al form stable corrosion resistant oxides,[5] (iv) P and B stabilize an amorphous phase when alloyed with iron,[7] and (v) N has been shown to improve pitting resistance in steels.[8] The elemental content of M50 is shown in Table I.

Table I. Elemental Composition of M50 Tool Steel (% by Wt.).

Carbon	0.85
Manganese	0.25
Silicon	0.20
Phosphorous	0.015 (max. allowable)
Sulfur	0.010 (max. allowable)
Chromium	4.00
Vanadium	1.20
Molybdenum	4.30
Iron	Remainder

II A. Simulation Tests

Laboratory field-service-simulation tests on implanted-M50 samples were designed to simulate the environment inside an engine bearing compartment. Figure 1 shows the arrangement of the test. The cylindrical surface resting on the flat side of the upright cylinder is intended to simulate a roller bearing-on-race contact geometry. The cylinders were positioned in place and totally immersed for 2 hr in a contaminated polyester oil. The oil was contaminated by adding three ppm (wt.) of chlorides as ASTM DD665 synthetic seawater to the oil and then adjusting the water content to a level of 600 ppm (wt.) by the addition of distilled water. This level of contamination was selected based on a NAPC evaluation of Naval Fleet oil samples.[9] The two parts were then removed from the oil and allowed to drip dry. A meniscus of contaminated oil was retained between the two parts, as shown in Fig. 1. This system was then exposed to alternate cycles of moist air at 60°C (8 hrs.) and 4°C (16 hrs.) for a period of several weeks. The test was developed[9] to simulate the corrosion mechanism which occurs in gas turbine engines.

The test shown in figure 1 was done for several implanted ions and several time periods. Figures 2-6 show the results of these tests in the form of photographs of

1. **Test pieces (both M50 alloy steel) were placed in contact as indicated by the dotted line.**

FLAT SURFACE
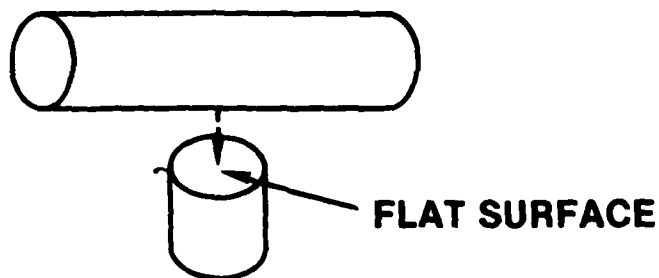
2. **Both pieces in place were immersed in chloride-contaminated oil for 2 hrs., removed, and allowed to dry.**

3. **A meniscus of contaminated oil was retained between the two parts:**

UPPER CYLINDER (end view)

CI-CONTAMINATED OIL
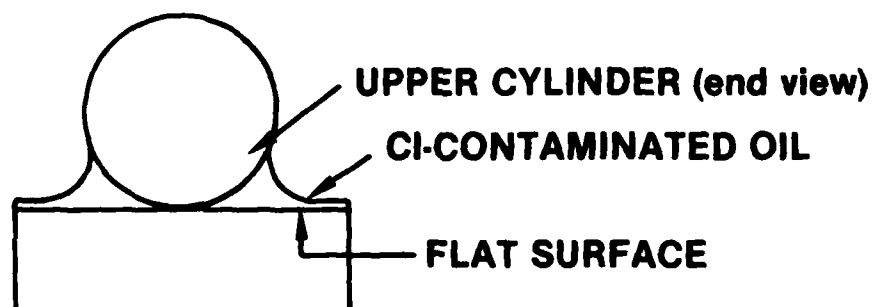
FLAT SURFACE

FIG. 1. Laboratory-simulated field service test of corrosion of bearings.

Con.   Virgin

4 wks.

Al   Al

FIG. 2. Optical photographs of the flat surfaces of M50 test samples after a 4 week simulated field service test. The two unimplanted samples at the top show pitting under the line of contact. The two Al implanted samples at the bottom show somewhat less pitting attack. (Magnification 10x).

4

Con.   Cr

4 wks.

Ti   Cr+P

FIG. 3. Optical photographs of the flat surfaces of M50 test samples after a 4 week simulated field service test. The unimplanted sample (upper left) shows pitting under the line of contact. The Cr and Cr+P implanted samples show complete immunity, and the Ti implanted sample shows very slight attack. Magnification 10x).
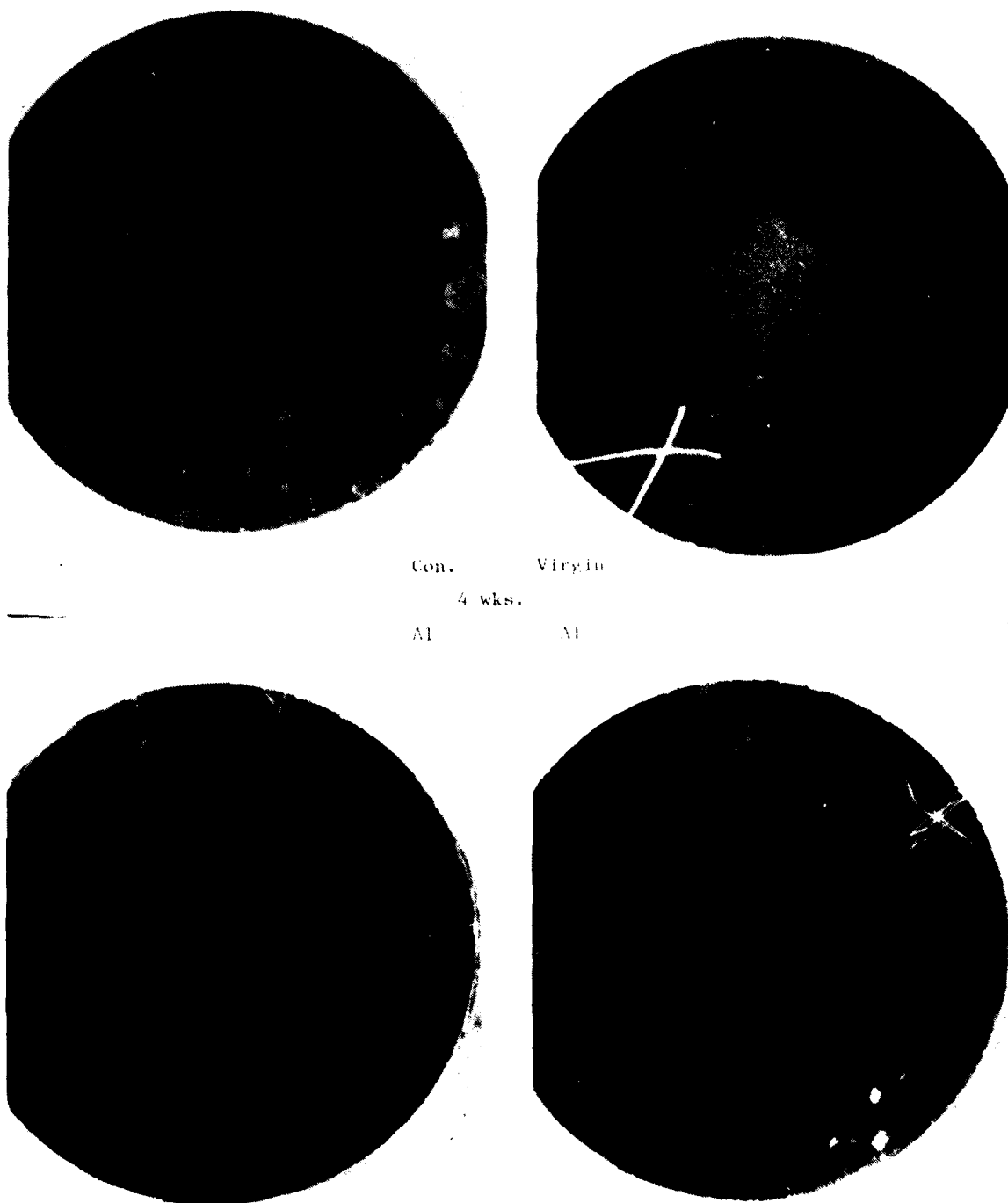
5

FIG. 4. Optical photographs of the flat surfaces of M50 test samples after a 5 week simulated field service test. The unimplanted sample at the top shows pitting under the line of contact. The Ti implanted sample shows a line of crevices beneath the line of contact. (Magnification 10x).

FIG. 5. Optical photographs of the flat surfaces of M50 test samples after a 7 week simulated field service test. The unimplanted samples at the top show pitting under the line of contact. The two Cr+Mo samples at the bottom show an improved resistance to general corrosion but a line of crevices beneath the line of contact. (Magnification 10x).

7

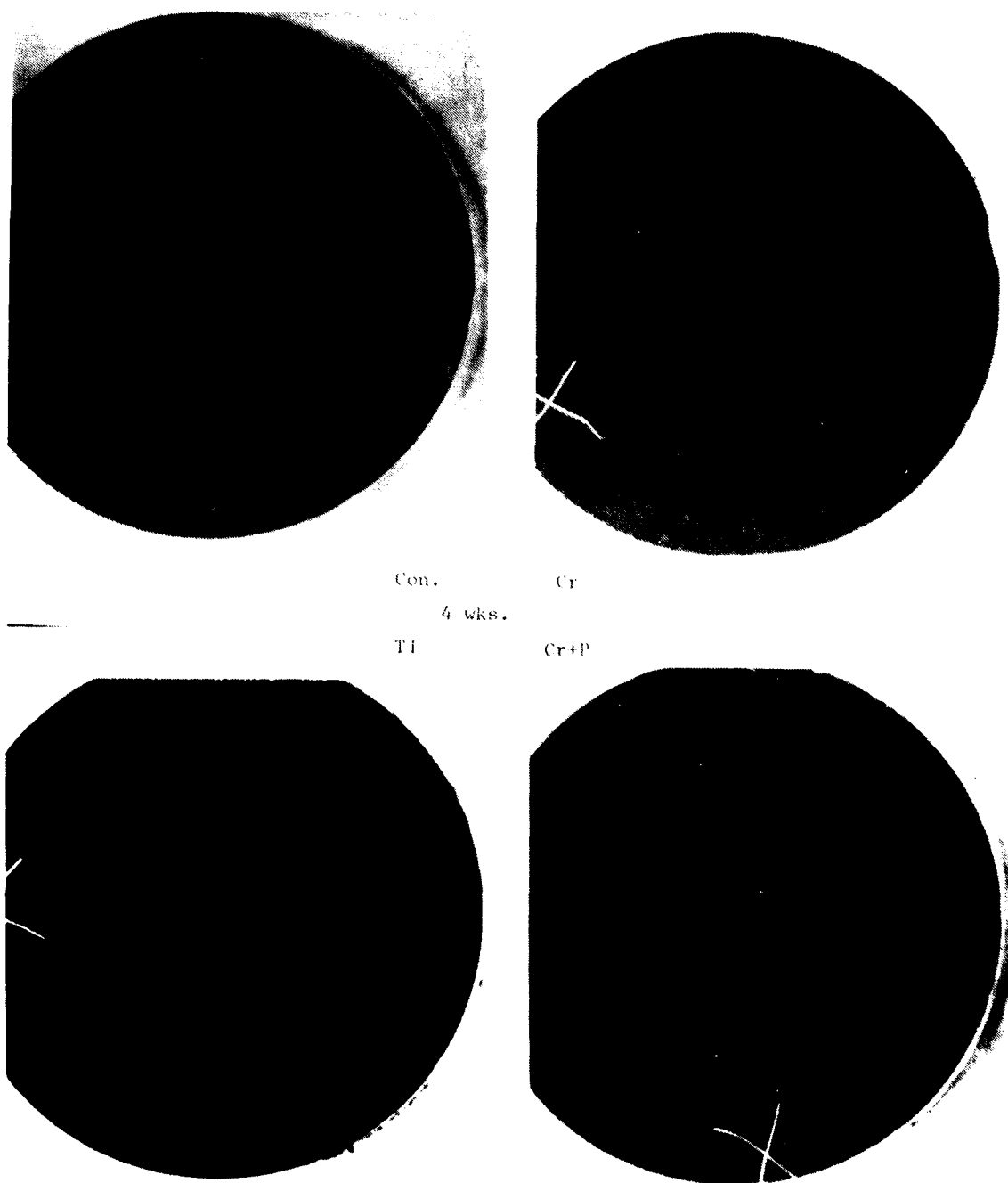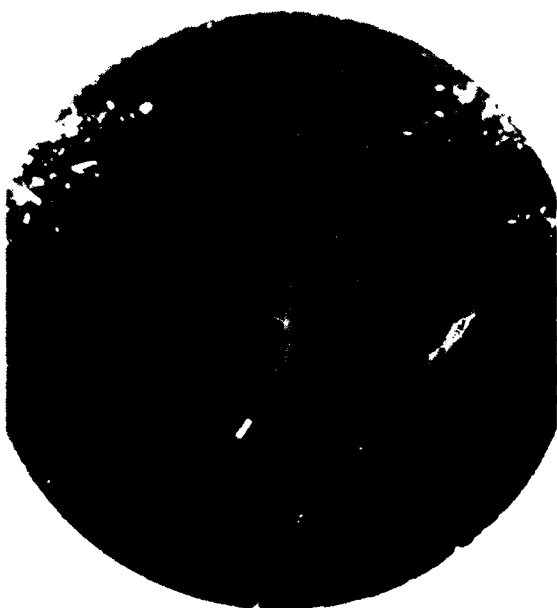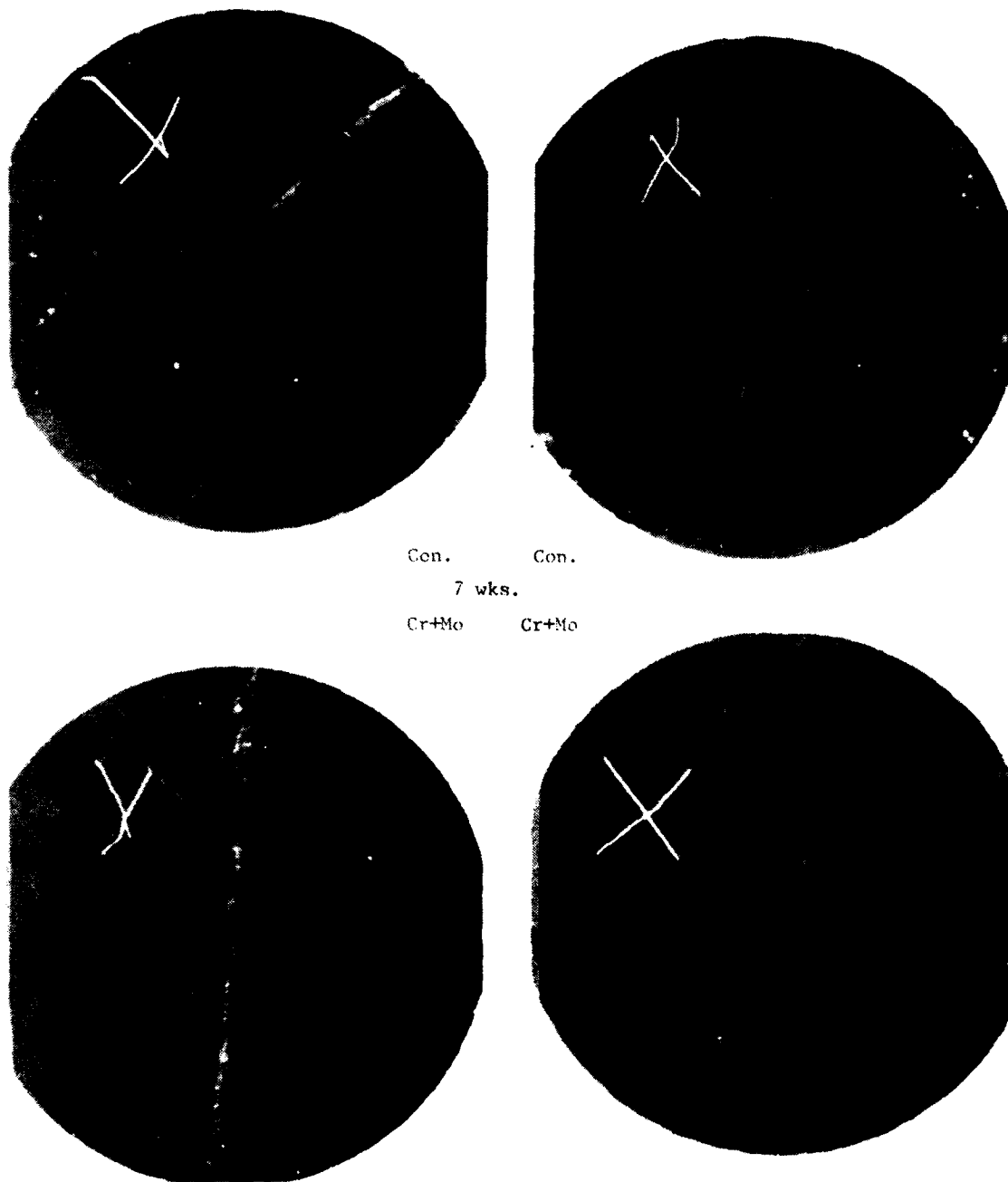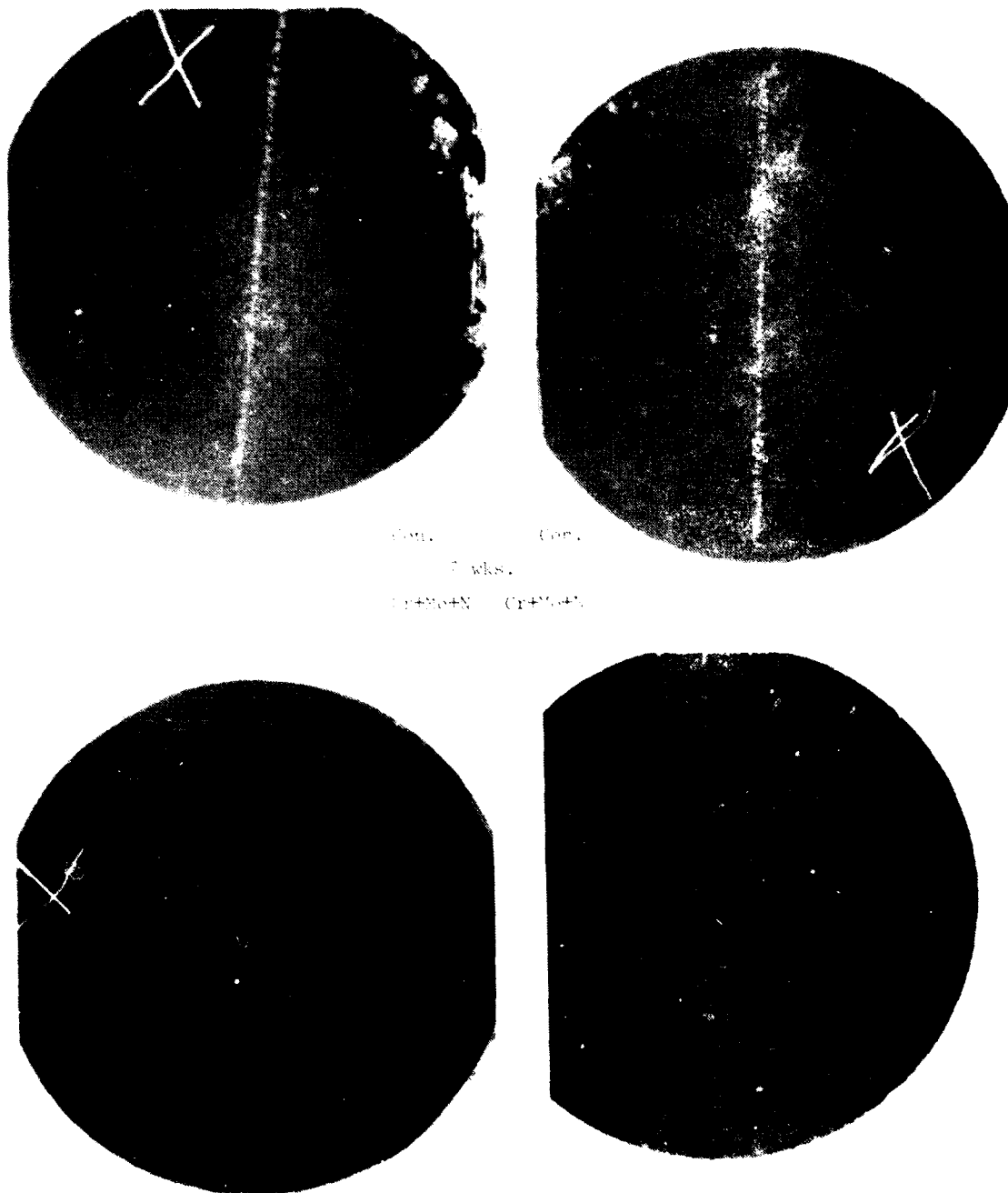FIG. 6. Optical photographs of the flat surfaces of M50 test samples after a simulated field service test. The two unimplanted samples at the top show pitting under the line of contact. The two Cr+Mo+N implanted samples at the bottom show complete immunity. (Magnification 10x).

scattered light from the flats at a magnification of 10 times. The highly polished specular samples appear dark in the absence of diffuse scattering from corrosion sites. The x's on some samples were purposely scratched to aid in focussing the camera. When the flat and cylindrical surfaces were unimplanted M50 alloy, there was severe corrosion after 4 weeks as shown in the upper left of figure 2. The attack generally occurs in two areas; e.g., a line of pits beneath the line of contact between the cylindrical and flat surfaces, and general corrosion in the thin layer of oil outside this region. The upper right hand side of Figure 2 is an unimplanted and uncorroded sample for comparison purposes. The bottom of figure 2 shows two samples identically implanted with Al and tested for 4 weeks. Only a very small improvement in corrosion resistance is noted. The fluences for the implanted species Al, Cr, and Ti were sufficient to enrich the surface with the implanted element to concentrations of 20% to 30 at.%. The upper left of figure 3 shows a control sample and the other samples are identified as Cr, Ti, and Cr+P implantations. In all three implanted cases there is a dramatic decrease in both general corrosion attack and pitting attack for a 4 week test. For the Cr+P implant there is virtually no corrosion attack.

Figure 4 shows the results for a high dose Ti implantation after a 5 week corrosion test. Note that the general corrosion is somewhat reduced, but there is still localized corrosion which is now in the form of a line of crevices rather than pits. Figure 5 shows the results for two identically implanted Cr+Mo samples and two controls after a 7-week test. The general corrosion is once again reduced by implantation, but as in the case of the 5-week Ti test, there is localized corrosion in the form of a line of crevices. Finally, in Figure 6 we have a 7-week test for two identically implanted Cr+Mo+N implants and two controls. This combination is very effective in improving the general and localized corrosion resistance. A qualitative ranking of the improvement in corrosion resistance produced by implanting ions or combinations of ions is listed in table II. Implantation conditions for all sample numbers may be found in the Appendix.

Table II. Ranking of results of simulated field service corrosion test.

Ions	Fluence $(\times 10^{17}/cm^2)$	Energy (keV)	Sample#	Test Duration (wks.)	Corrosion Inhibition
Cr+ P	1.5 0.5	150 40	31579	4	very good
Cr+ Mo+ N	1.5 0.5 0.1	150 100 12.5	31579	7	very good
Cr	1.5	150	61169	4	very good
Ti	2.0	55	4379	4	fair
Ti	2.0	55	4379	5	fair
Cr+ Mo	1.5 0.5	150 100	31579	7	poor
Al	0.6 1.0	50 100	32979	4	poor

II B. Electrochemical Tests

Two independent electrochemical characterizations were done to study two types of corrosion behavior. Passivity tests in strong acids provide insight to general corrosion (rusting) behavior, and pitting tests in buffered chloride ion solutions give a measure of the resistance to localized corrosion (pitting).

The acid tests were done in 1 Normal H_2SO_4 at room temperature. Potentiodynamic scans in the anodic direction produce a characteristic curve such as that shown as the solid line in Figure 7 for an ideal case. From open circuit voltage OCV (i.e., no imposed voltage) the potential is scanned in the positive direction at 1 mV/s and the current increases quickly (active behavior) which corresponds to metal dissolving from the surface. As the potential increases further, the current abruptly drops and the surface is said to be passivated by a thin oxide film. Resistance to general corrosion is associated with the width and height of this active-passive behavior. The dashed curve shows the desired result for improved corrosion resistant ion implanted surfaces. That is, lowering of the maximum current, and a narrowing of the active region. Both effects are indications that the surface is more easily passivated, and that improved corrosion resistance may be expected. Figure 8 shows the results for unimplanted M50 and for Cr, Mo, Ti, and Cr+Mo implanted[3] M50. Notice that all implanted samples show a reduction in the maximum current density. These tests establish a qualitative ordering of the improvement to be expected in general corrosion behavior which is (from best to worst) Cr+Mo, Cr, Mo, Ti, unimplanted M50.

The chloride ion tests were in a pH6, 0.01 or 0.1 Molar NaCl, buffered solution. The buffer ensured that the pH was constant throughout the measurements. The salient points of these measurements are illustrated in idealized curves in Figure 9. The solid line in the upper portion of Figure 9 represents the potentiodynamic scan that is obtained in a Ph6 solution with no Cl ions added. From open circuit voltage, the potential is scanned in the positive direction producing a constant but small current flow. In this region, the rate of metal dissolution is very small and the metal is said to be passivated. At higher potential the sharp rise in current is caused by pitting or transpassive behavior, the latter not being important to this discussion. Adding chloride ions produces the dashed curve. The Cl-ions locally attack the passive film producing pits where metal ions are actively dissolving and cause increased current flow. The breakdown potential E_b characterizes the metals' ability to withstand pitting attack. The bottom portion of the figure demonstrates the desired result of surface treatment (e.g., to drive the breakdown potential back toward more positive values). The difference in breakdown potentials for implanted versus unimplanted samples is a measurement of the pitting behavior of materials.

Figure 10 presents potentiodynamic polarization curves for a 0.1M NaCl solution for several implantations[5]. Notice that all implantations improved the breakdown potential, and that Cr+Mo offered the best protection. Table III lists the breakdown potential E_b for the samples run in 0.1M NaCl solution. The qualitative order of effectiveness is, from best to worst, Cr+Mo, Cr, Mo, Ti.

FIG. 7. Idealized potentiodynamic polarization scan (current versus voltage characteristic) for a ferrous alloy in 1 Molar H_2SO_4 at room temperature. The dashed line indicates an improvement in the passivity of the surface and therefore improved corrosion resistance.

11
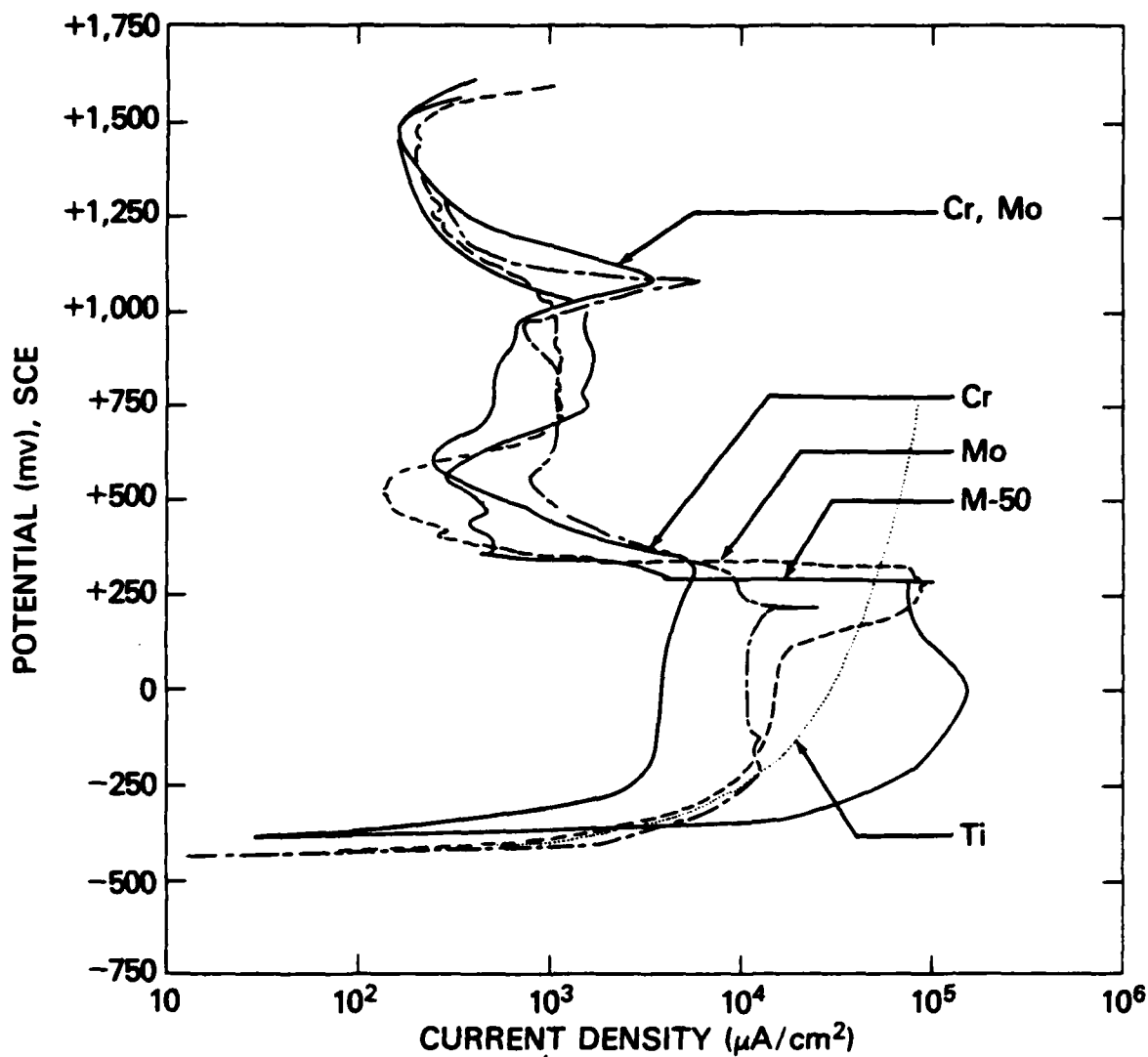
FIG. 8. Potentiodynamic anodic polarizaiton data produced in hydrogen-saturated 1N H_2SO_4 for M50 steel, and for M50 steel implanted with titanium chromium, molybdenum and chromium + molybdenum.
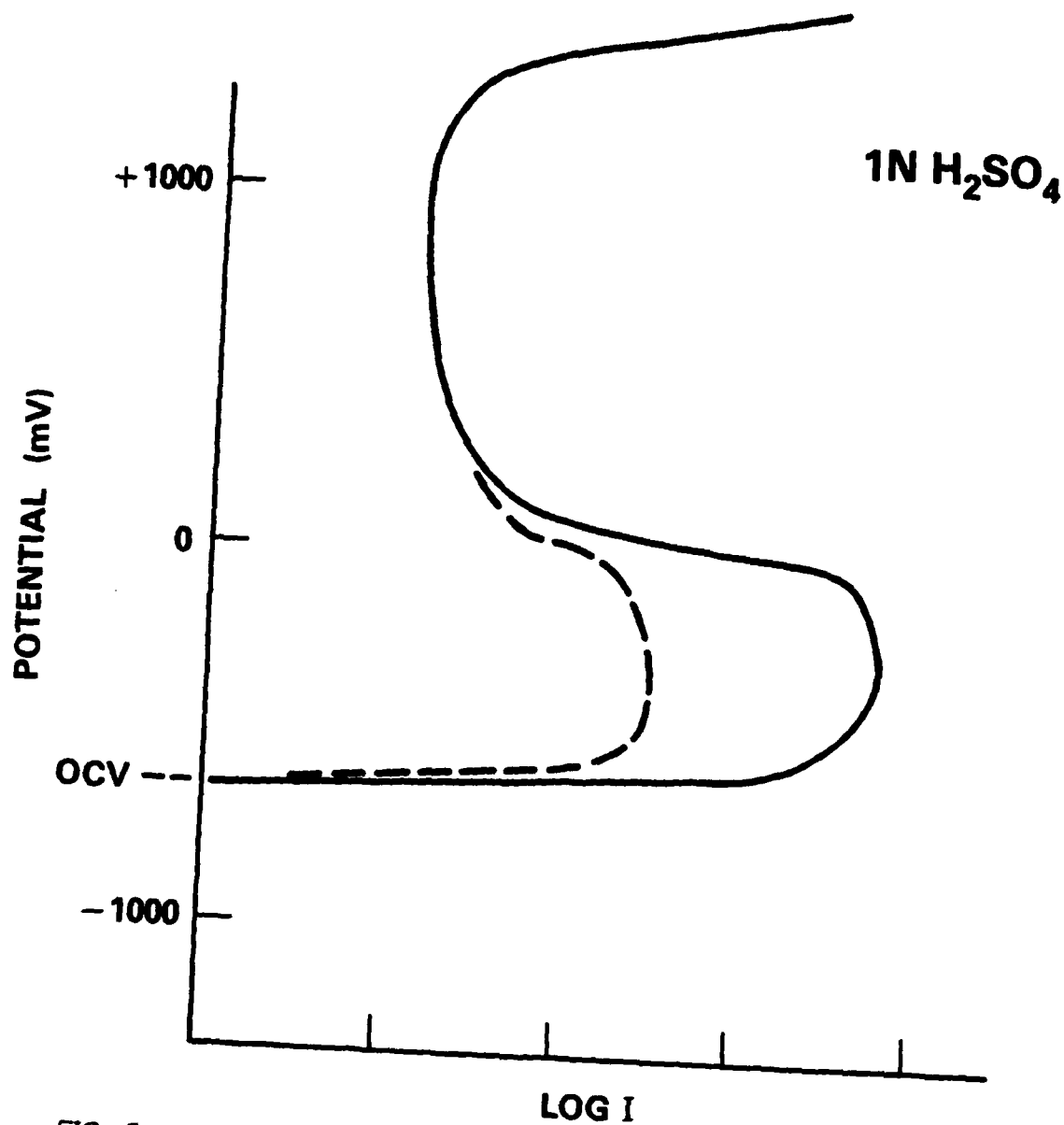
12

0.01M NaCl
Ph6, BUFFERED
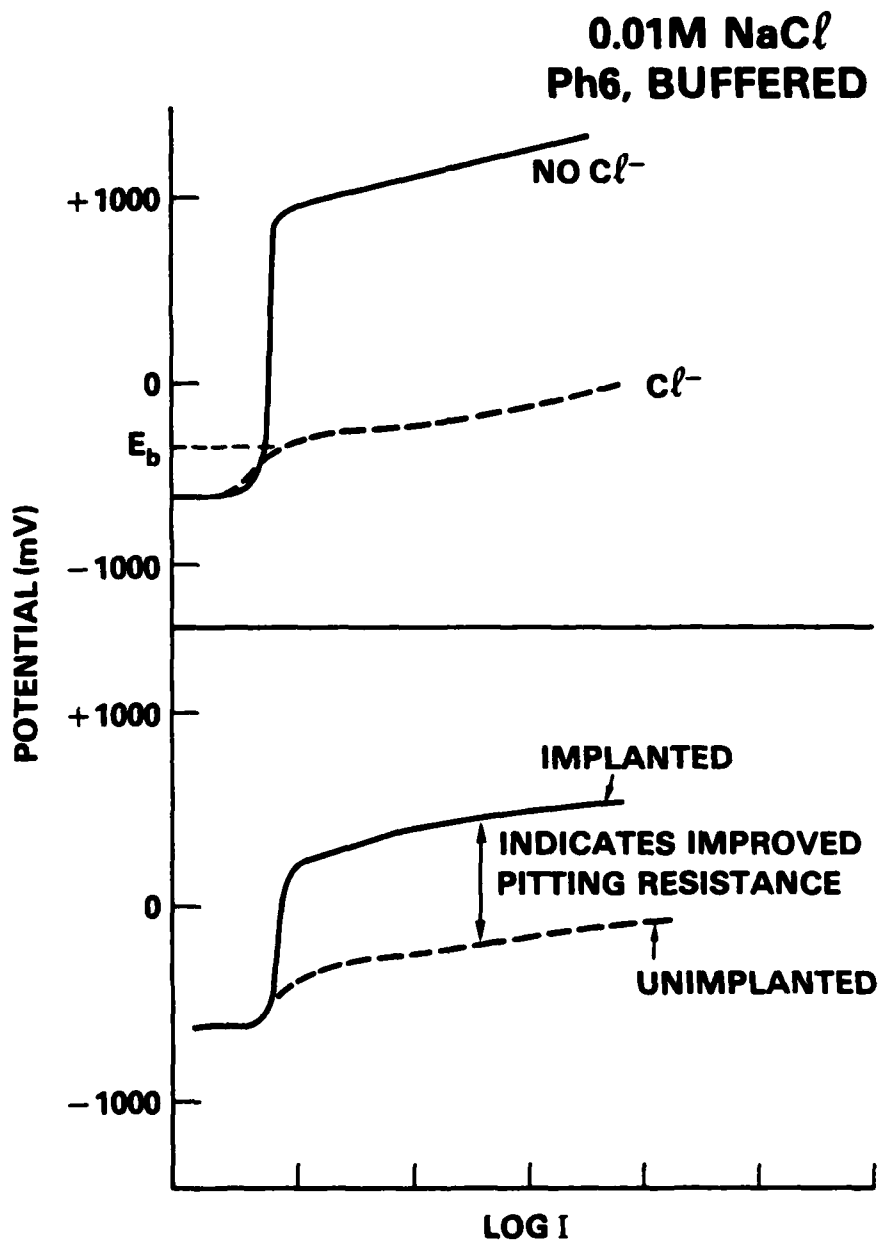
FIG. 9. Idealized potentiodynamic polarization scans (current versus voltage charactersitic) for a ferrous alloy in a buffered pH 6 solution at room temperature. The upper set of curves demonstrate the effect of adding Cl⁻ ions to the solution. E_b defines the pitting potential where a sharp increase in current results when pits form on the surface. The lower set of curves demonstrate the desired result of ion implantation, i.e., force the pitting potential toward higher values.

13

FIG. 10. Potentiodynamic anodic polarization data produced in buffer solution of pH6 containing 0.1 M NaCl for M50 steel, and for M50 steel implanted with titanium, chromium molybdenum and chromium + molybdenum.

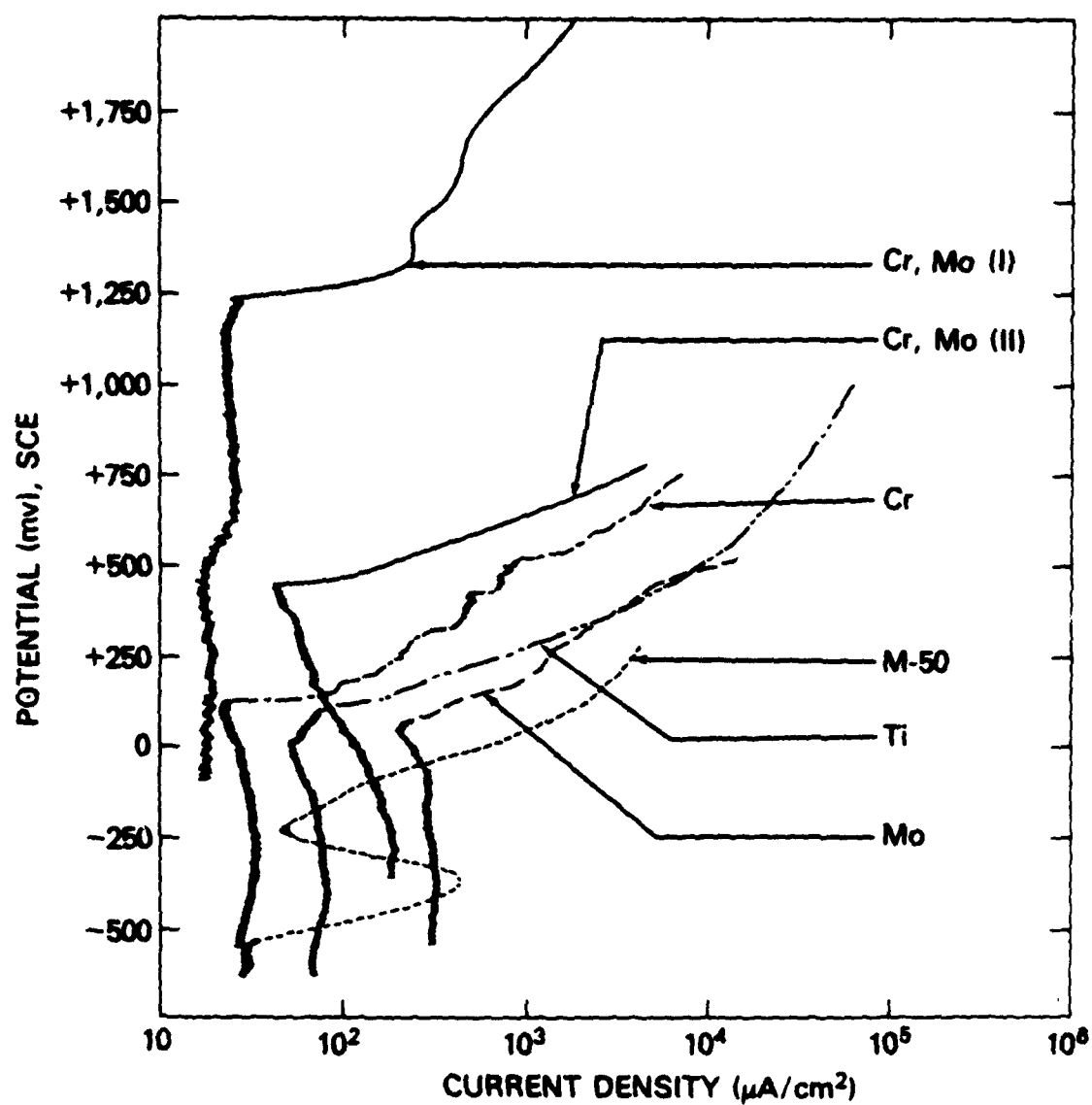Table III. Breakdown potentials in 0.1M NaCl solution for M50 steel implanted with various ions.

Ion(s)	Fluence $(\times 10^{17}/cm^2)$	Energy (keV)	Sample#	E_b (mV)
Cr+	1.5	150	2879	+1250
Mo	0.5	100		
Cr+	1.5	150	2879	+ 450
Mo	0.5	100		
Cr	1.5	150	2779	+ 130
Mo	0.5	100	31979	+ 60
Ti	2.0	55	111578	0
M50	---	---	------	- 230

The pitting data in a 0.01M NaCl solution for several implanted species are listed in Table IV. Two different pretreatments were examined. In one case, the sample was polarized positively immediately upon immersion into the solution so that the air formed film was being tested for pitting. In the other case, the air formed film was removed by polarizing in the negative direction (H_2 charging) for 15 min, then scanned positively allowing a new passive film to form. The latter was the pretreatment for the 0.1M data in Table III as well. The former is more realistic since it is the treatment an actual implanted bearing would receive.

Notice that Cr implants appear to be better than Cr+Mo implants in this test, since Cr has higher breakdown potentials.

Table IV. The breakdown potentials, E_b, in 0.01M NaCl solution for M50 steel implanted with various ions.

Air Formed Film

Ion(s)	Fluence $(\times 10^{17}/cm^2)$	Energy (keV)	Sample#	E_b(mV)
Cr+ P	1.5 0.5	150 40	31579	+700
Cr	4.0	150	42079	+650
Cr	2.0	150	82779	+570
Cr+ Mo	2.0 0.35	150 100	12180	+430
M50	---	---	------	+290
N+ Cr+ Mo	0.2,0.32 1.5 0.5	25,50 150 100	2579	+270
Cr+ Mo	2.0 0.35	150 100	82779	+250

H$_2$ Charged

Ion(s)	Fluence $(\times 10^{17}/cm^2)$	Energy (keV)	Sample#	E_b(mV)
Cr	2.0	150	82779	+700
Cr+ P	1.5 0.5	150 40	31579	+500
Cr	4.0	150	42079	+350
Cr+ Mo	2.0 0.35	150 100	12180	+330
N+ Cr+ Mo	0.2,0.32 1.5 0.5	25,50 150 100	2579	+200
M50	---	---	------	+180
Cr+ Mo	2.0 0.35	150 100	42079	+170
Cr+ Mo	2.0 0.35	150 100	42079	- 10

Examining the data for 5 different corrosion tests including, (i) simulation tests, (ii) 1-normal H_2SO_4 test, (iii,iv) the 0.1M and 0.01M NaCl pitting tests with cathodic charging, and (v) the 0.01M pitting test on air formed film, we can draw some tentative conclusions. Table V provides a qualitative ranking of the effectiveness of ions for each test. Cr and Cr+Mo implants are common to all tests. Chromium implants show good performance in all tests, while Cr+Mo appears high in two tests and low in three. Also, Cr+P performs very well in the tests in which it was studied. Therefore, Cr, Cr+Mo, and Cr+P were selected for further examination in full scale rolling element bearings.

Table V. M50 Corrosion Test Data (Qualitative Ranking).

Sim.	IN H_2SO_4	0.1M NaCl (cath.)	0.01M NaCl (no cath.)	0.01M NaCl (cath.)
Cr+P	Cr+Mo	Cr+Mo	Cr+P	Cr
Cr	Cr	Cr	Cr	Cr+P
Cr+Mo+N	Mo	Mo	Cr+Mo	M50
Ti	Ti	Ti	M50	Cr+Mo+N
Cr+Mo	M50	M50	Cr+Mo+N	Cr+Mo
Al				
M50				

II C. Physical Characterization of Implanted Surfaces

The elemental composition of Cr and Cr+Mo implanted samples was investigated with nuclear reaction profiling[10] (NRP) and Rutherford Backscattering (RBS) analysis. The NRP method is capable of giving quantitative concentration versus depth distributions for Cr in heavier (i.e., Fe) metal hosts, and RBS gives quantitative distributions for the heavier Mo in lighter hosts. Figure 11 shows the Cr profile for a fluence of 2×10^{17}/cm^2 and implant energy of 150 keV where the Cr concentration is greater than 20 at.% over the first 500 angstroms (2 microinches) of material. Profiles such as these are instrumental in optimizing implantation parameters. For example, the initial Cr and Mo fluences chosen for these experiments were 1.5×10^{17}/cm^2 and 0.5×10^{17}/cm^2, respectively. NRP chromium profiles indicated that the surface concentration of Cr was depleted by sputtering from 20 at.% to 12 at.% after the Mo implantation, the latter being marginal for good (i.e., stainless steel like) corrosion properties. Therefore the implantation parameters were changed to 2×10^{17}/cm^2 for Cr and 3.5×10^{16}/cm^2 for Mo. NRP and RBS profiles show that for the latter conditions the Cr surface concentration is 20 at.% and the Mo concentration is 8 at.% over the first 300 angstroms.

Information on the longevity of the implanted layer has been obtained by optical, SEM, and x-ray fluorescence data on Cr-implanted rolling-contact-fatigue specimens. In this test conducted at NAPC two identical rings with a 14 inch crown radius contact one another and are loaded as shown schematically in figure 12. Several rings were implanted to 1×10^{17} and 2×10^{17} Cr/cm^2 at 150 keV on two different 1" long segments along the circumference. One implanted ring was tested against an unimplanted ring for each of 3 conditions -- (i) pure rolling, (ii) rolling plus 7% slip, and (iii) rolling plus 14% slip. The test is run with an oil jet directed at the conjuction of the rollers as shown in figure 12.
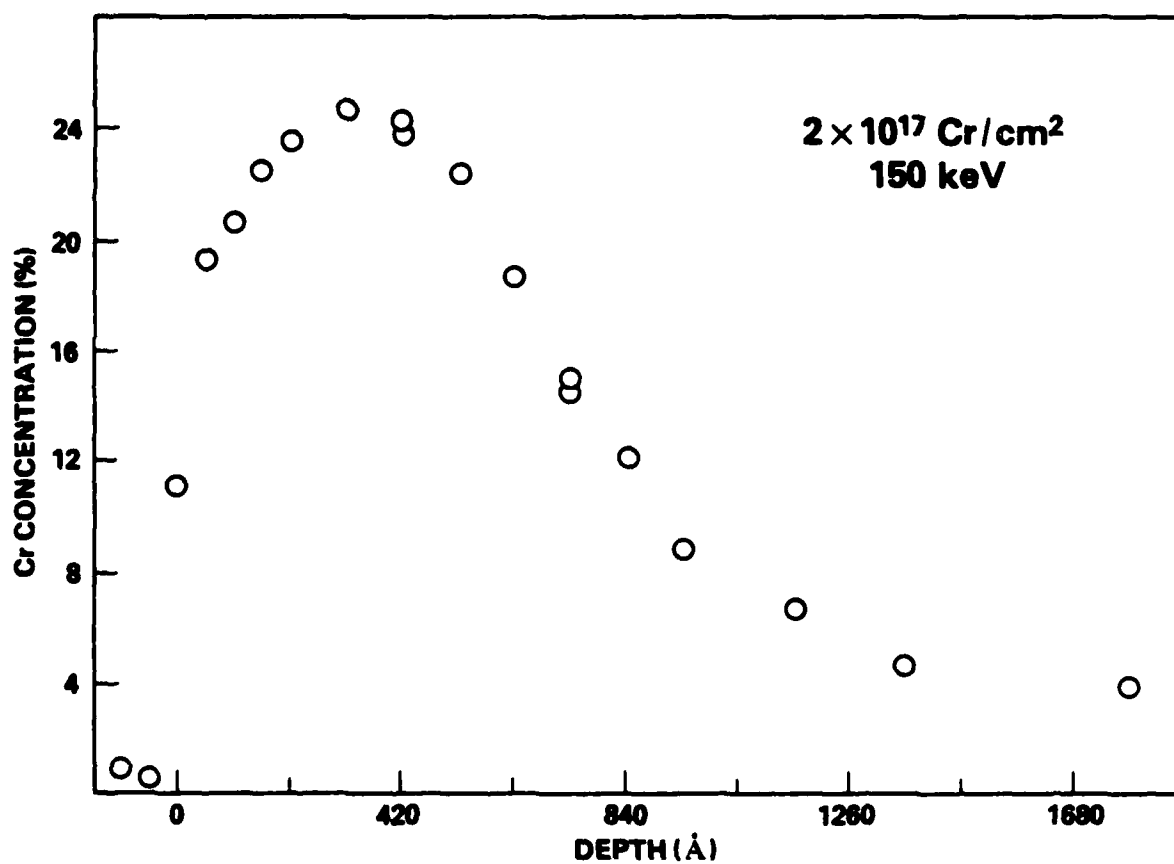
FIG. 11. Nuclear (p,γ) Resonance Profile of Cr in M50 tool steel. The Cr was
ion implanted to a fluence of 2×10^{17} ions/cm^2 at an energy of 150 keV.
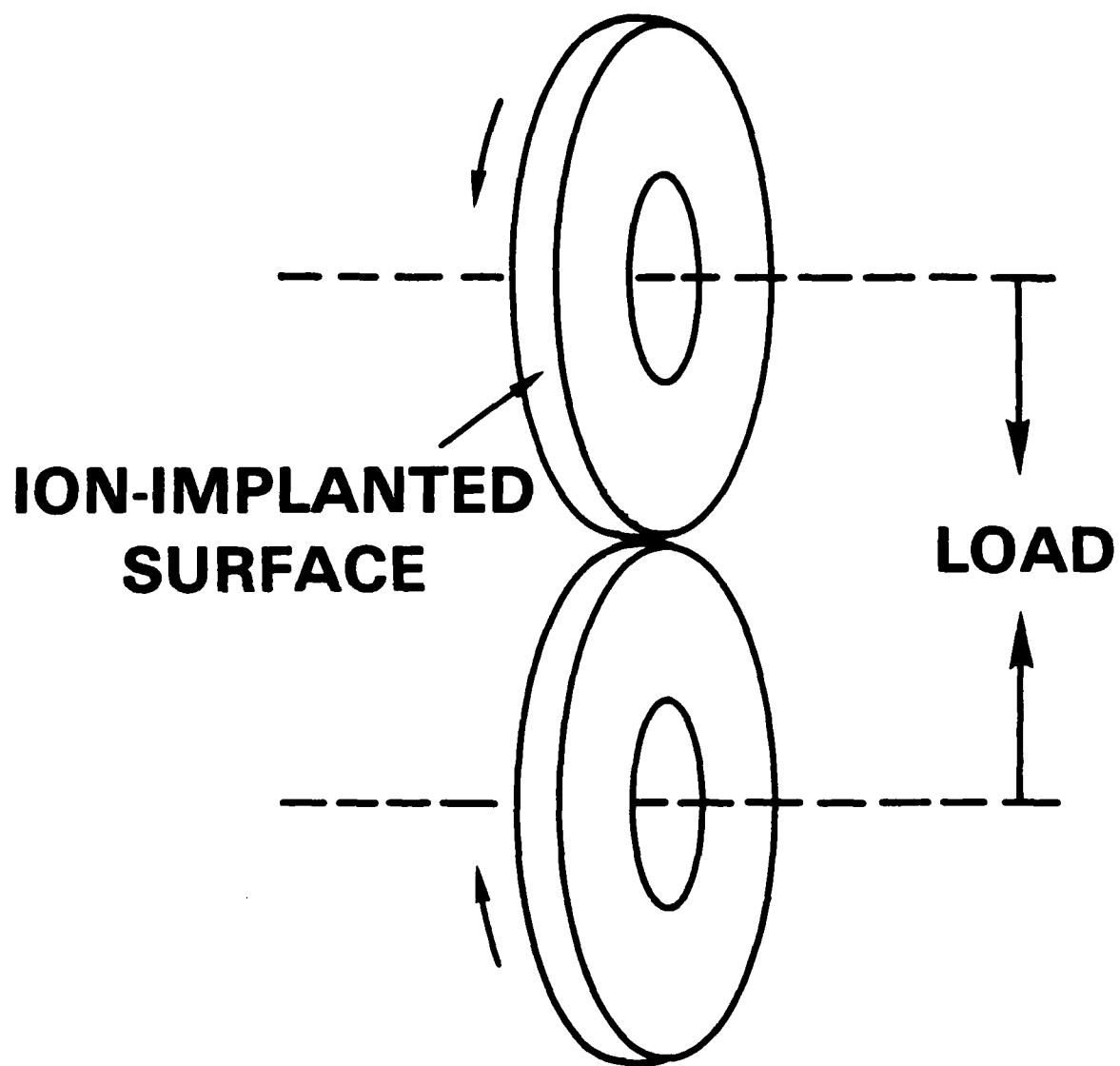
ION-IMPLANTED SURFACE

LOAD

FIG. 12. Schematic diagram of rolling contact fatigue test geometry.

19

For pure rolling and 7% slip, no discernible wear occured on either the implanted or unimplanted areas on the rings after a test of 100 hours at a load which resulted in a maximum Hertzian stress of 185 ksi. The appearance of the pure rolling and 7% slip rings before and after testing are shown in the upper left hand optical photograph in Figure 13 at a magnification of 81x. For the 14% slip specimens, the unimplanted area has worn such that the original machining marks have disappeared leaving a pitted surface caused by fatigue spalls. This unimplanted worn region is shown in the upper right of Figure 13 and should be compared with the $1 \times 10^{17}/cm^2$ Cr implanted surface (lower left) and the $2 \times 10^{17}/cm^2$ Cr implanted surface (lower right). The latter shows a significant improvement over the unimplanted case as evidenced by notably lower wear seen by the retention of the machining marks.

SEM photographs at a magnification of 200x are shown in Figure 14. The upper left is the 14% slip sample in an unworn area and the upper right is in the unimplanted wear area. Lower left is the $1 \times 10^{17}/cm^2$ Cr implanted and worn surface and the lower right is the 2×10^{17} Cr implanted and worn surface. The machine marks are much more numerous in the $2 \times 10^{17}/cm^2$ Cr implanted sample than for the unimplanted area showing that much less wear has occured. The SEM micrographs were obtained for an electron energy of 20 keV and a tilt angle of 30°.

The same samples were examined with energy dispersive x-ray analysis equipment on the SEM to ascertain the Cr content in and out of wear scars. The upper left of Figure 15 is an x-ray spectrum for an unimplanted, unworn M50 ring. The x-ray peaks are identified, from left to right, as Mo_L (between 0 and 4 kev), $V_{k\alpha}$, $Cr_{k\alpha}$, $Cr_{k\beta}$, $Fe_{k\alpha}$, $Fe_{k\beta}$ (between 4 and 8 kev). All x ray spectra were normalized with the $Fe_{k\beta}$ line at 8 vertical boxes. The $Cr_{k\alpha}$ line is 3.5 boxes tall for both unimplanted unworn (upper left) and unimplanted worn (14% slip, upper right) surfaces and is the Cr x-ray signal originating from the 4% Cr content in the bulk M50 alloy. The lower left spectrum is for the $2 \times 10^{17}Cr/cm^2$ as-implanted sample. The Cr x-ray signal here is 9 boxes tall. The lower right spectrum is from the worn area of the $2 \times 10^{17}Cr/cm^2$ sample and has a Cr peak 5.8 boxes tall. The x ray spectra were taken at a 100x magnification so that a large number of machine marks and wear pits are averaged over. From these x-ray spectra one concludes that the x-ray analysis technique is quite sensitive to implanted Cr in approximately the first (0.1 μm) 1000 angstroms even though the excitation volume of the incident 20 keV electrons is about 1 μm. Moreover, a significant fraction of the implanted Cr remained in the surface after prolonged wear testing. These characterizations also suggest a possible beneficial effect on wear. However, more work is necessary to define any positive wear effects and these wear samples are being tested for their electrochemical behavior.

III. Implantation of Bearings

The bearings of concern in this work are a $2\frac{1}{2}$" diameter roller bearing from a T58 engine used in a H46 helicopter, and a 9" diameter mainshaft ball bearing from a J79 engine used in F4 aircraft, and bearings from a T63 gas turbine. The number of bearings that have been implanted are listed in Table VI along with pertinent information on bearing size and function of each mechanical test. The implant conditions are similar for those listed in Table IV for the same ions.

There are a number of practical problems to be considered for the successful implantation of the bearings. Obviously, all contacting surfaces must be implanted to protect against the pit-initiated fatigue failure mechanism. This entails implanting the

FIG. 13. Optical photographs of surfaces of rolling contact fatigue samples at a magnification of 81x. Upper left is appearance of pure rolling and 7% slip samples before and after testing in either the implanted or unimplanted condition. Upper right is 14% slip unimplanted sample and shows that original machining marks have been removed. Lower photographs are for $1 \times 10^{17}/cm^2$ left and $2 \times 10^{17}/cm^2$ right Cr implanted samples, 150 keV tested with 14% slip and these show some what less wear.
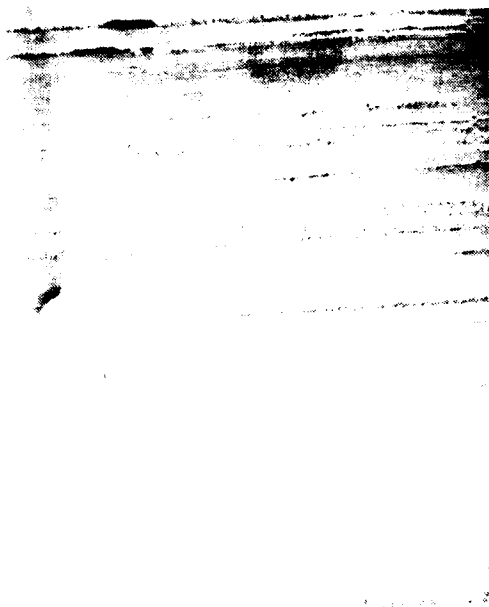
FIG. 14. SEM micrographs at a magnification of 200x of rolling contact fatigue samples. Upper left is a micrograph of an ion implanted 14% slip sample taken on an unworn area. The upper right is an unimplanted 14% slip sample. The lower micrographs are of the worn area for 14% slip samples implanted with 1×10^{17} Cr/cm^2 (left) and 2×10^{17} Cr/cm^2 (right) at 150 keV.
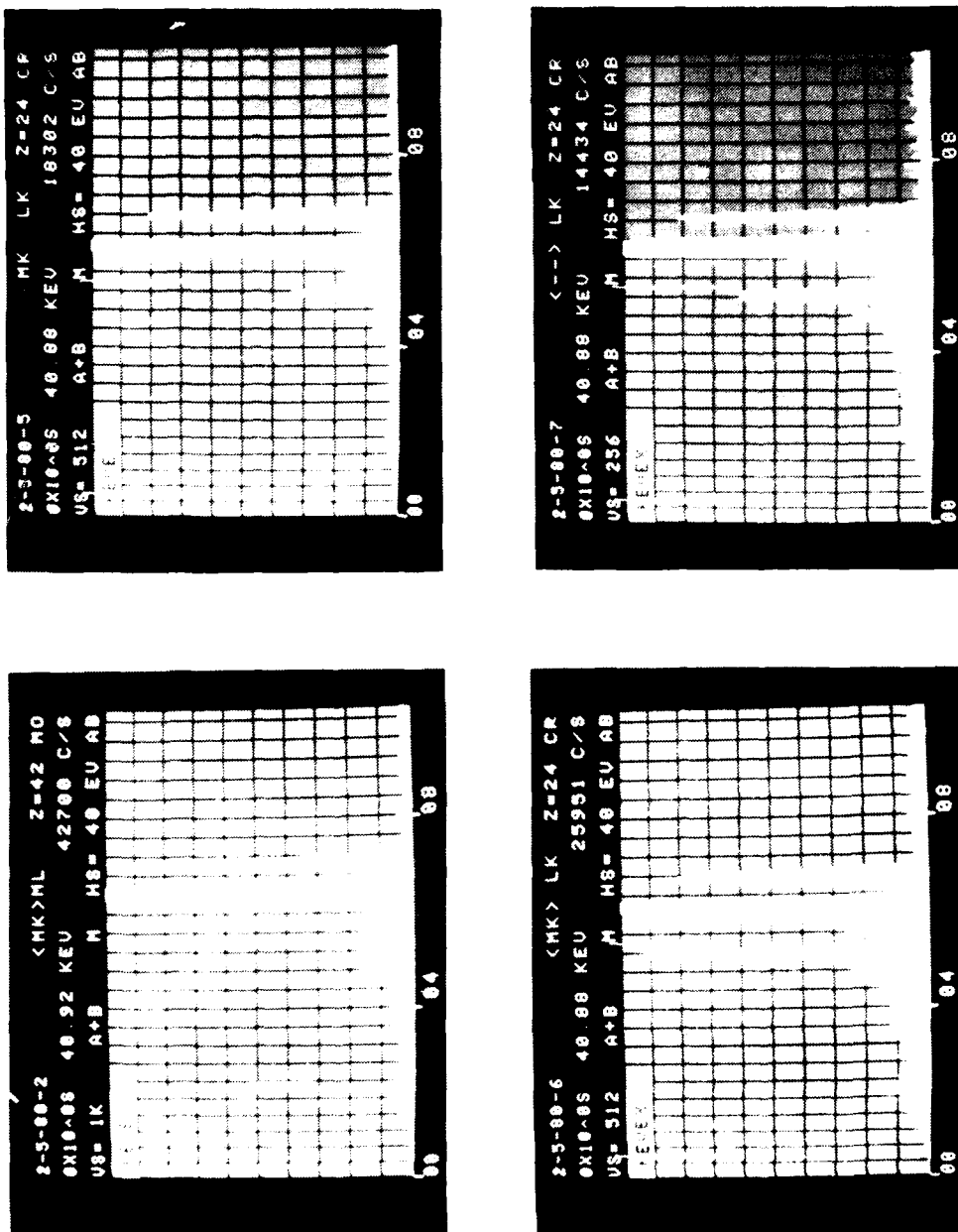
FIG. 15. X-ray spectra taken on selected areas of rolling contact fatigue samples. All spectra are normalized with the Cr K_β line at 8 vertical boxes. Upper left is as received M50 with the Cr K_α line at 3.5 boxes. The Cr K_α line for the 14% slip unimplanted sample shown in upper right is also 3.5 boxes. The lower left is for a 2 x 10^{17} Cr/cm^2 150 keV implant in the unworn condition (9 vertical boxes) and the lower right is for an implanted and worn area (14% slip) and the Cr peak is 7.8 vertical boxes.

23

TABLE VI

BEARINGS SELECTED FOR IMPLANTATION

Application	Type*	Bearing Size - mm			No. Brgs. Implanted	Ions	Function in Program
		O.D.	Bore	Rolling Element Size			
J79 Gas Turbine Engine Thrust Bearing	B	225	150	22.22 (Ball)	1	Cr+Mo	Performance and Field Evaluation
T58 Turboshaft Engine - No. 4 Bearing	R	68	40	7 long x 7 dia.	2	Cr+Mo	Performance and Field Evaluation
Modified T58 Bearing	R	68	40	7 long x 7 dia.	10 / 11	Cr+P / Cr	Fatigue Endurance Testing
T63 Gas Turbine Engine Bearing No. 3 / No. 6	B / R	55 / 42	30 / 25	6 (Ball) / 5 long x 6 dia.	2 / 2	Cr+P	T63 Engine Evaluation in a Test Cell with Contaminated Oil

*B = Ball Bearing
R = Roller

24

active surfaces of the bearing (i.e., the inner race, outer race, and the total area of the rollers and the balls). In order to implant the bearings in a reasonable period of time, sufficiently intense beam currents of these unconventional ion species were developed and used.[11] For Cr a typical beam current is 500 µA at 150 keV. This is 75 watts of power incident on the bearing which must be dissipated or the bearing will overheat, causing loss of hardness. Fortunately, M50 holds its hardness well in that it has been established that no loss of hardness occurs at temperatures of 800°F for 1000 hrs.[12] This enables the heat dissipation to be handled in some cases by radiation losses alone.

For the races the beam was scanned vertically but not horizontally so that the beam irradiated the bearing races over the vertical extent of the race (1.5 cm for T58; 3 cm for J79) with a width of about 1 cm. All the races were clamped tightly to a solid aluminum or brass plate and rotated at 1.5 rpm. Typically 60 revolutions were required to finish one race. In this manner, heat was transferred to the plate and both the plate and race then radiated the heat away. Table VII shows the maximum temperature of each bearing component during implantation. The vacuum was typically less than 3 x 10^{-6} Torr during implantation and the target chamber was always vented to atmospheric pressure with dry nitrogen gas after the bearing components had cooled to under 550°F.

Table VII.   Normal and maximum temperatures reached by bearing components during implantation.

Component	Temperature (°F)	
	T_{Normal}	T_{Max}
J 79 inner race	400	500
J 79 outer race	400	500
J 79 ball	450	500
T 58 inner race	400	550
T 58 outer race	500	640
T 58 roller	390	650

Figures 16, 17, 18, and 19 are photographs of the jigs used to implant the races.

The T58 rollers (0.275" tall x 0.275" diam.) were implanted on the ends with the jig shown in Figure 20. A stainless steel frame held down to an aluminum block contains the rollers which are held tightly in place by a stainless bar pressed against the roller array by two screws. Beneath the rollers is a thin sheet of Mo. Cooling is accomplished by fastening the holder with three screws to a water cooled shaft. Indium foil pressed between the aluminum block and cooled shaft promotes heat conduction from the block. The materials of stainless steel and Mo were chosen to minimize the effects of sputtering of the holder material onto the bearings. Brass and aluminum, which conduct heat much better than stainless, unfortunately sputter very efficiently and would therefore nonuniformally coat the rollers with Cu, Zu, and Al. Mo has a low sputtering coefficient and is considered innocuous at worst in that the small amount of sputtered Mo contamination on the bearings might even have beneficial effects on corrosion resistance. Impurities sputtered onto the bearings from stainless steel are chiefly iron, chromium, and nickel which also are compatible with the corrosion prevention purpose of the implanted layer. The sputtering coefficient for P on these materials is much smaller than for Cr and thus was not considered a problem.

Roller circumferences were implanted in four steps with the jig shown in Figure 21. Stainless steel water cooled tubing supports horizontal stainless struts each of
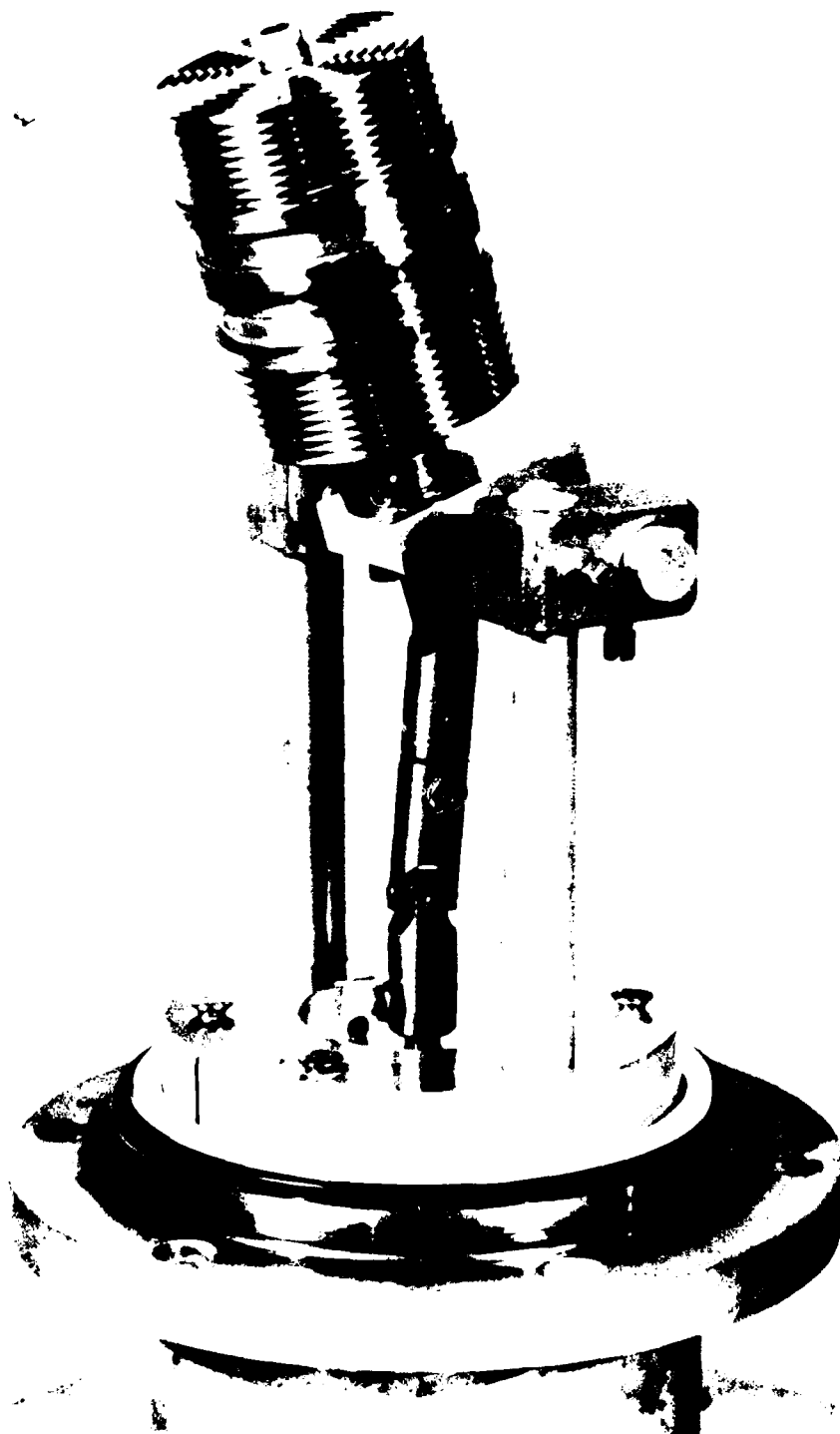
FIG. 16. Fixture for implanting two T58 bearing inner races. The material of the upper and lower holder is brass that is finned for more effective radiative cooling.
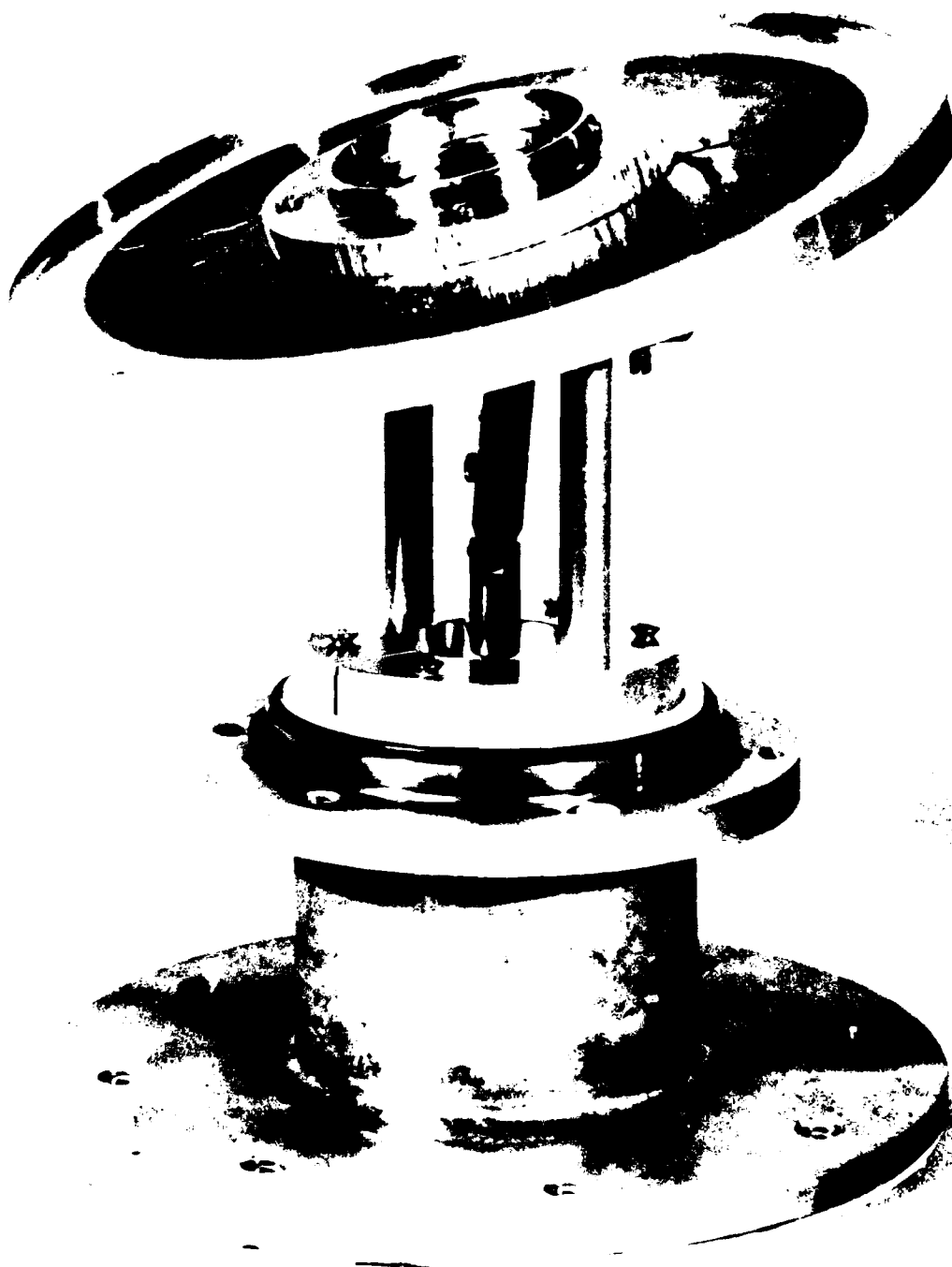
FIG. 17. Fixture for implanting one T58 bearing outer race. An aluminum clamp is screwed down to an aluminum plate which acts as a heat sink and also doubles as a fixture to hold the J79 bearing outer race.
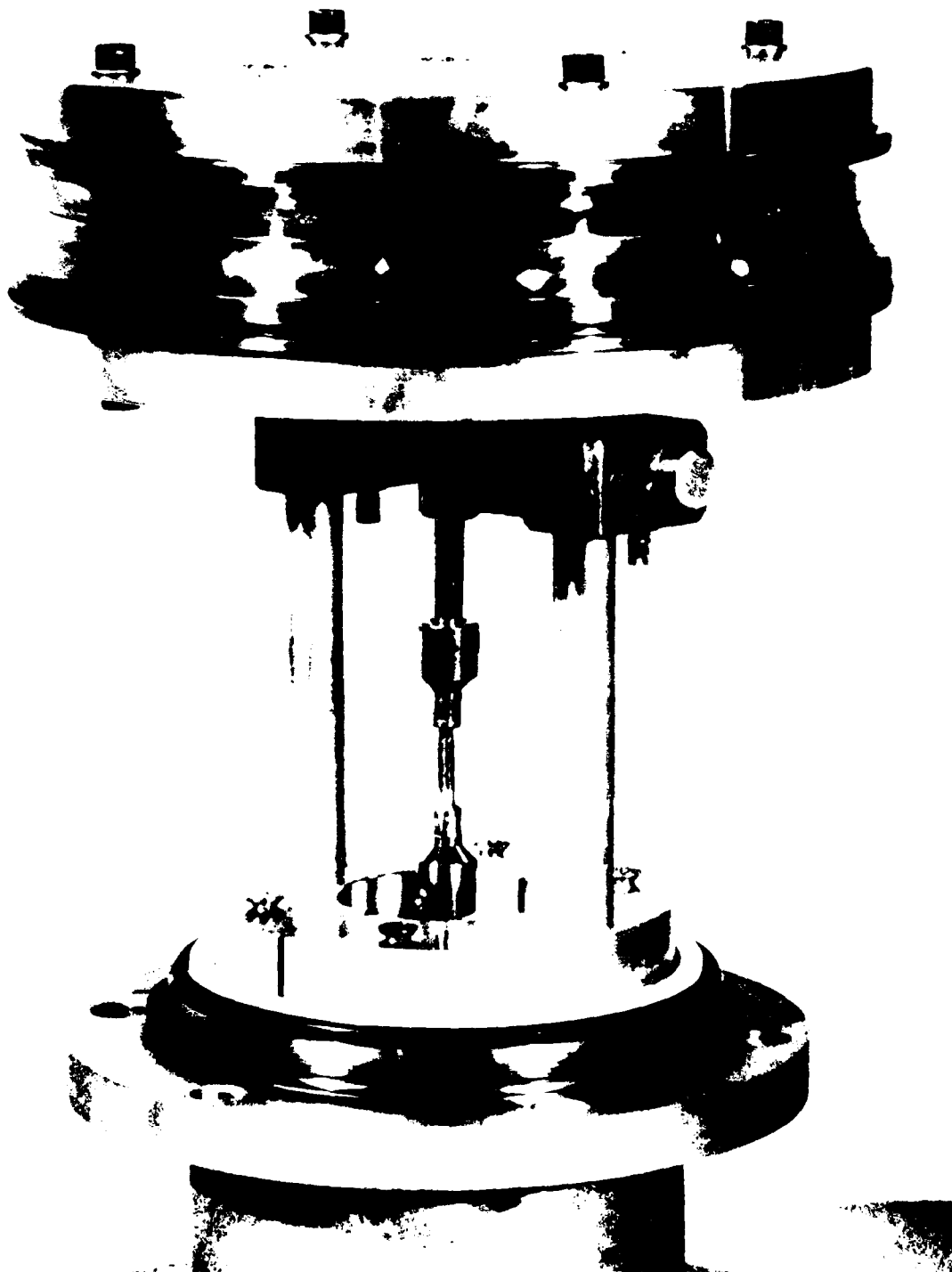
FIG. 18. Fixture for implanting J79 bearing split inner race. The upper and lower retaining plates are made of aluminum and they act as a heat sink.
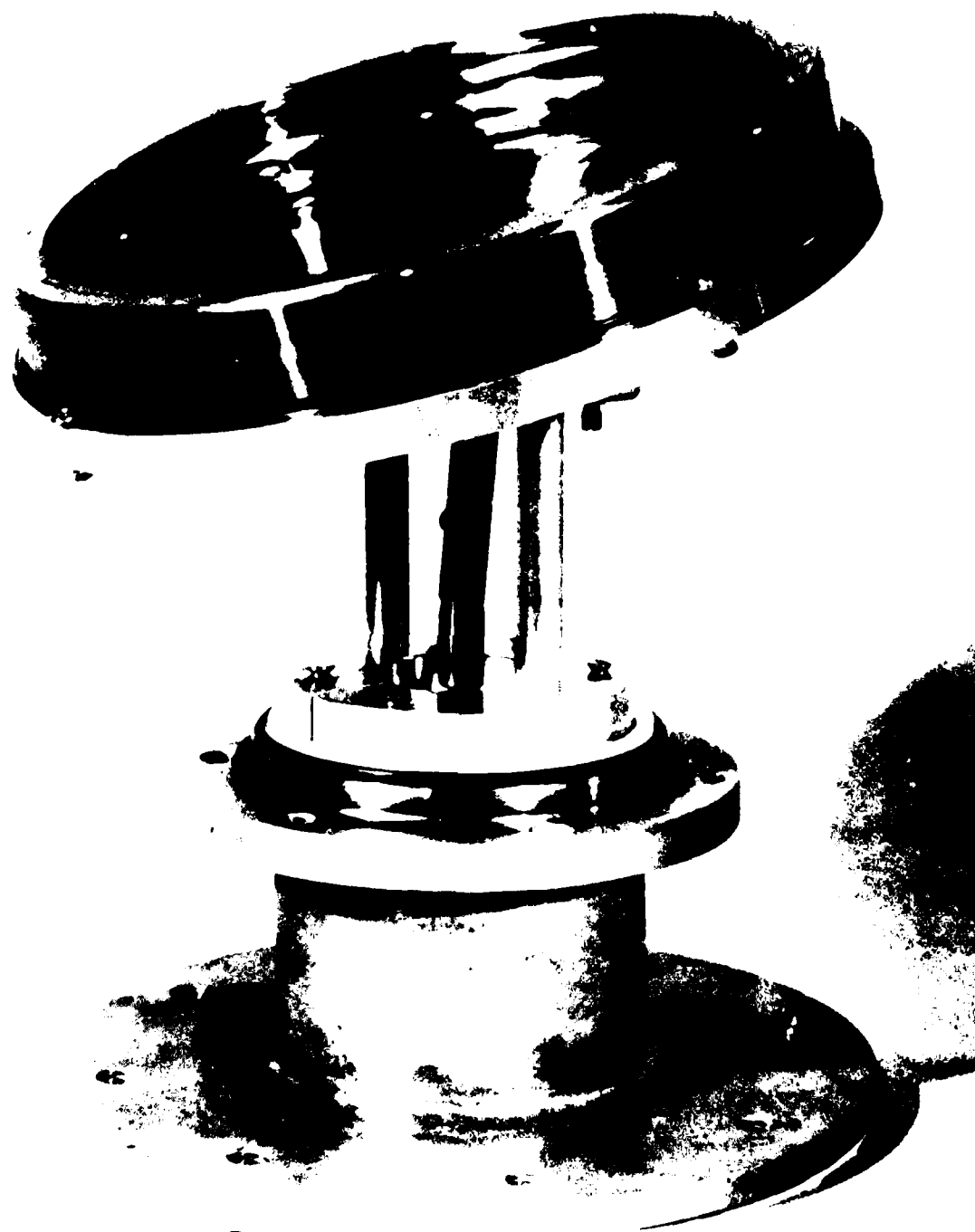
FIG. 19. Fixture for implanting 3/4 bearing outer race. The race is clamped to an aluminum base which acts as a heat sink.
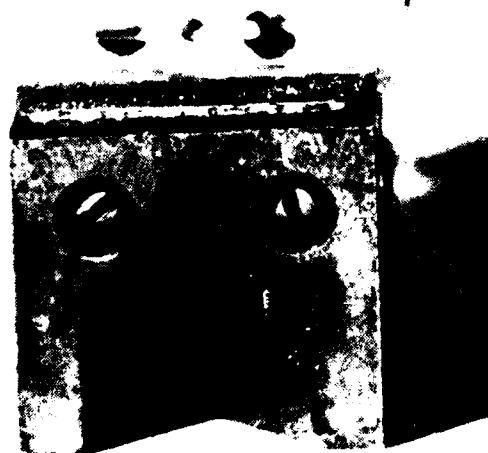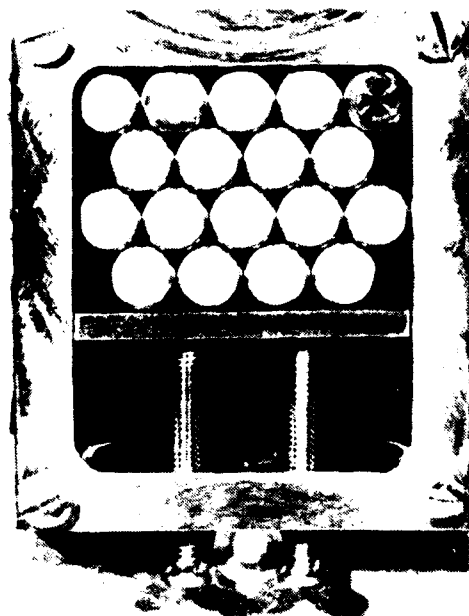
FIG. 20. Photograph of implantation jig used to implant 18 T-58 bearing roller ends. Stainless steel frame is turned over to implant opposite ends of rollers. The aluminum base is water cooled.
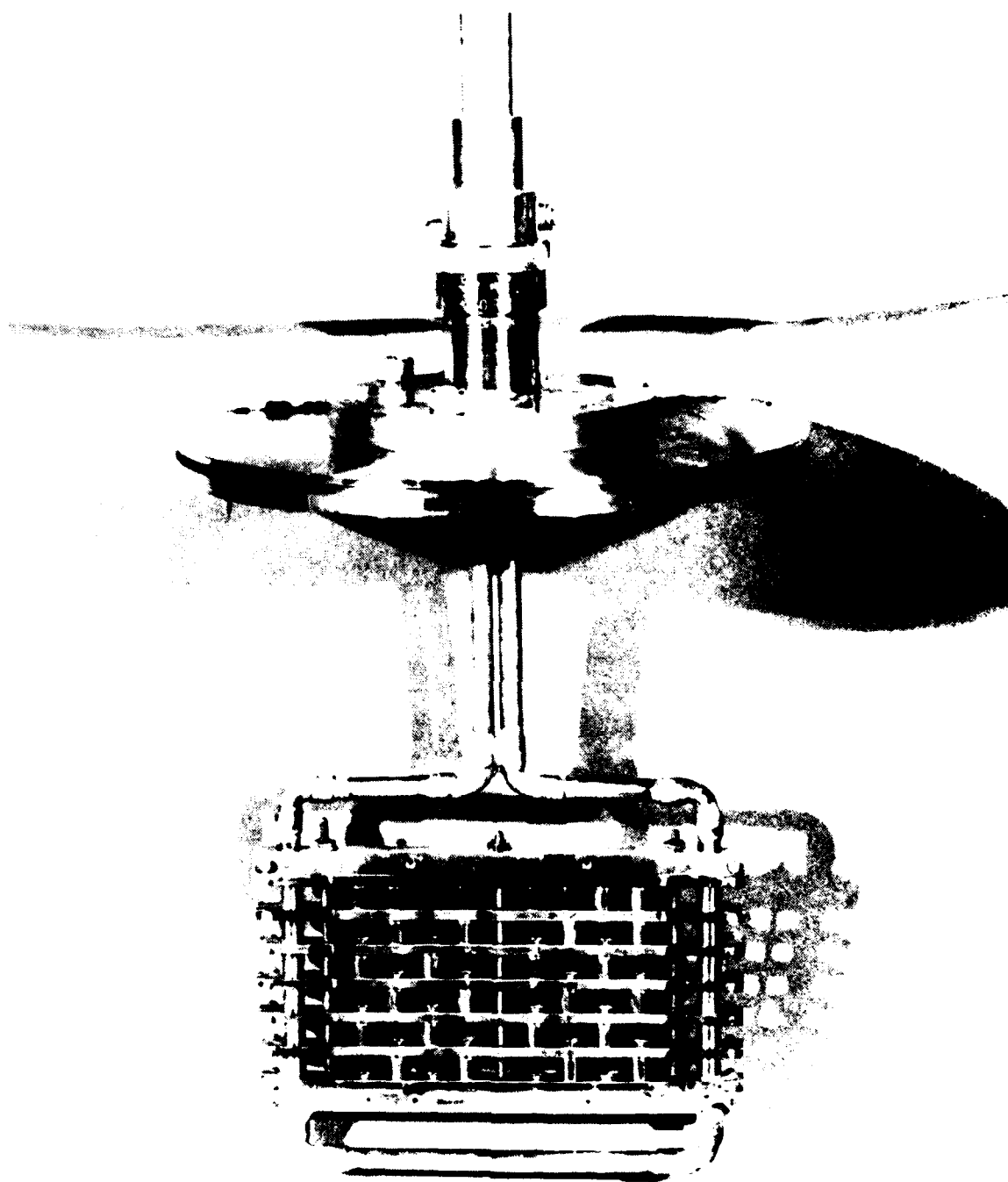
FIG. 21a. Photograph of implantation jig used to implanted up to 48 T-58 rollers at one time. One-quarter inch copper tubing provides water cooling and support for stainless steel bars that retain the rollers. Rollers are implanted in four rotations, 90° apart, for complete coverage of the circumference.
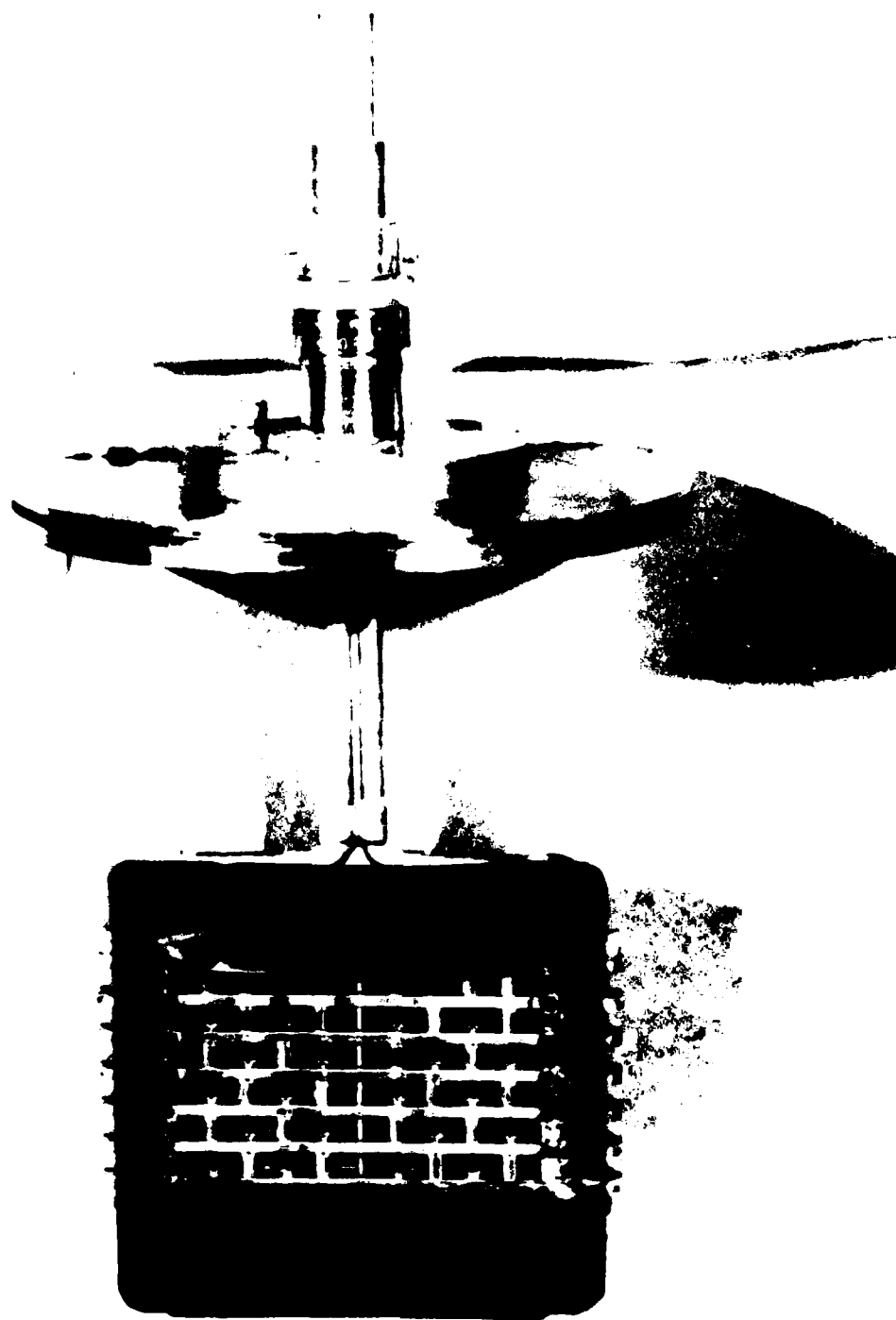
FIG. 21b. Same jig as in Figure 21a but with the sputtering shield installed which limits the amount of sputtering of holder material and supports.

which hold 8 rollers. The roller circumferences are implanted to a given fluence in four directions each at an angle of 45° to the holder. This implantation geometry results in a 30% calculated variation in fluence around the circumference of the roller. For the Cr implantations the fluence varies between 1.5×10^{17} and $2.1 \times 10^{17}/cm^2$. We have observed that the corrosion inhibition effects of Cr implantations for fluences between 1×10^{17} and $2 \times 10^{17}/cm^2$ are the same when measured by the simulation test mentioned previously. Therefore, the 30% variation in fluence is not expected to be a problem. This observation is also consistent with the well known observation that an abrupt improvement in the corrosion resistance of steels occurs at a Cr concentration of 12%, so that if this criteria is met by the lowest fluence implant, additional Cr will not substantially further improve the corrosion resistance.[5]

Figure 22 shows a planetary gear jig designed to implant up to 48 J-79 balls in one operation. It is shown set up for 24 balls on a 7.5 inch diameter. The 7/8" diameter balls are held in place by gravity in a stainless steel "golf tee" and each ball rotates 18.5 times for each rotation of the whole assembly. The beam is scanned horizontally and vertically over an area 7/8" high by 2" wide so that at any one time slightly more than 2 balls are being irradiated. The problem of temperature rise is solved by a 12 to 1 duty cycle wherein each ball is irradiated for about 3 seconds and allowed to cool (chiefly by radiation) for about 37 seconds.

The emissivity of the balls was determined by measuring the heating curve of a ball with a thermocouple attached to it in vacuum. Figure 23 presents the data for two different input powers of an Ar ion beam. From the equation in figure 23 and knowing the input power and surface area of the ball, an emissivity of 0.25 is computed. From this information we computed an equilibrium temperature of $390^\circ F$ for a 200 μA, 150 keV, beam. The measured value for the above implantation conditions was $425^\circ F$ which is in good agreement with the calculated value. During implantation the temperature of the bearings was measured and continuously monitored by means of an infrared pyrometer sighted on the bearing through a quartz window in the implantation vacuum chamber.

The procedure for implanting the balls with Cr was to implant in a cylindrical geometry to a fluence of $1 \times 10^{17}/cm^2$, rotate the balls 90° with respect to the vertical direction and implant again to a fluence of $1 \times 10^{17}/cm^2$. This leaves the surface with two poles containing $2 \times 10^{17}/cm^2$, two poles containing $1 \times 10^{17}/cm^2$, and the remainder of the surface with fluences between these values. This factor of two nonuniformity in fluence will not be deleterious for the same reasons as discussed for roller bearings.

IV. Performance and Endurance Testing of Bearings

One each of the J79 and T58 engine bearings (first two bearings listed in Table VI), were performance tested for 400 hours at conditions simulating speed, load, and temperatures of actual operating engines.

In addition, 10 each of the modified T58 bearings (Table VI) implanted with either Cr+P or Cr were fatigue endurance tested. Another group of 10 untreated bearings, also fatigue endurance tested, provided a baseline for comparison. All thirty bearings were made from a single lot of M50 steel and were manufactured at the same time. Differences in endurance life could therefore be attributed to the implantation process only since the material and manufacturing processes were statistically similar among the three groups.

33
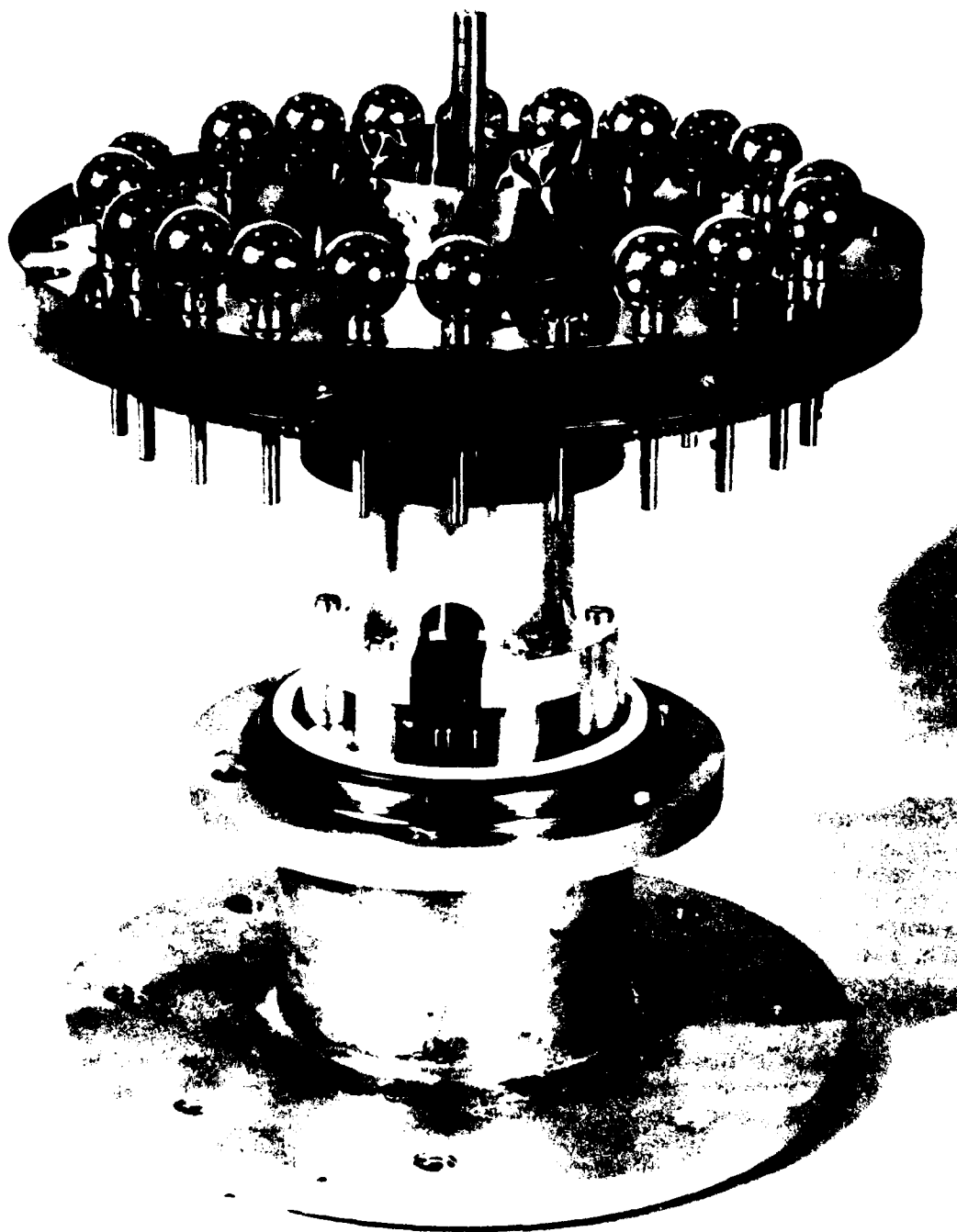
FIG. 22a. Photograph of planetary gear fixture used to implant 24 J-79 balls at one time (expandable to 48 balls). Stainless steel "gat free" retain the balls and each ball rotates through the beam spot which remains fixed at the dimensions 7/8" tall by 2" wide. A ball rotates 18.5 times for each rotation of the platform.
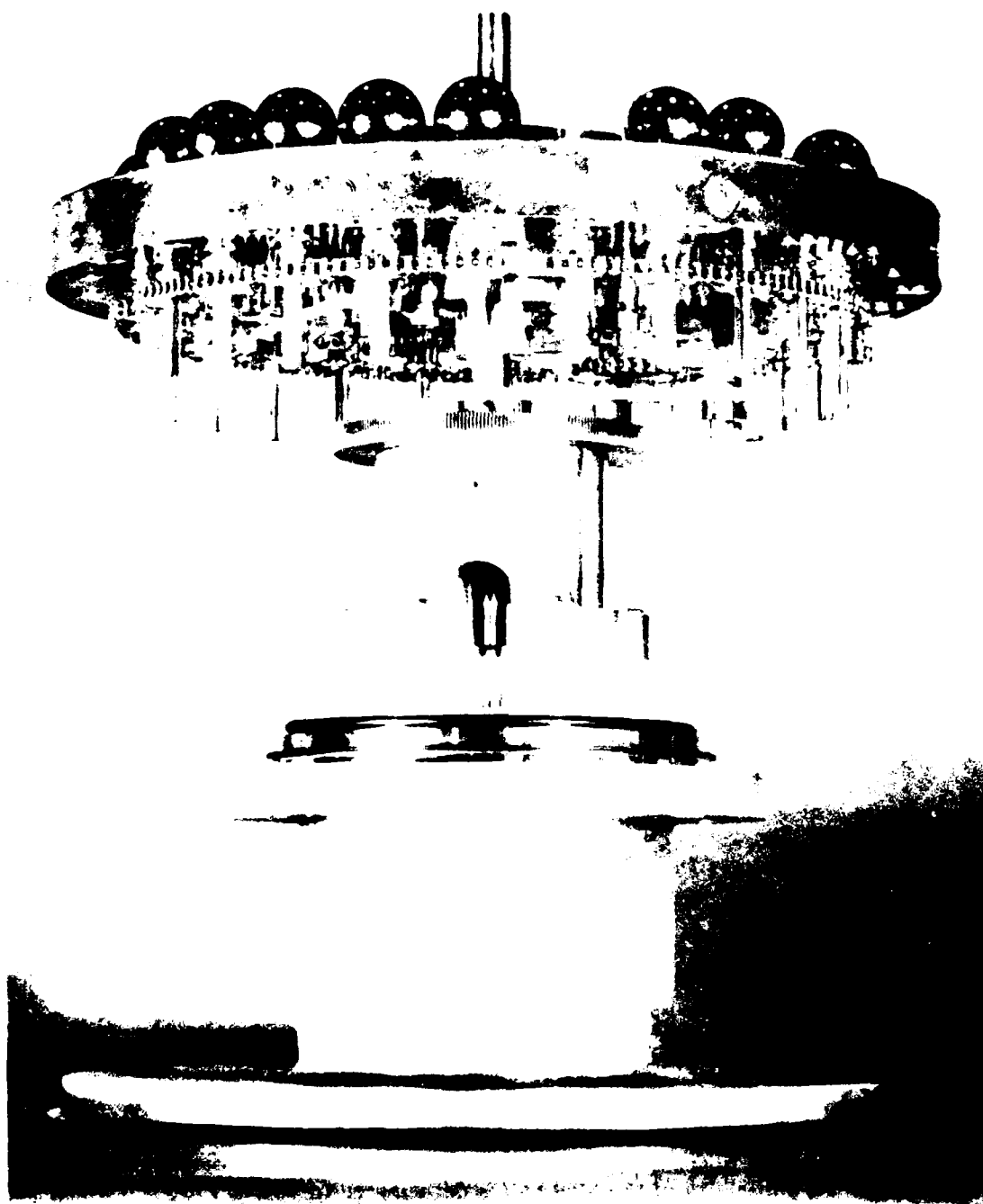
FIG. 22b. Same jig as in Figure 22a as viewed from beneath rotating platform.
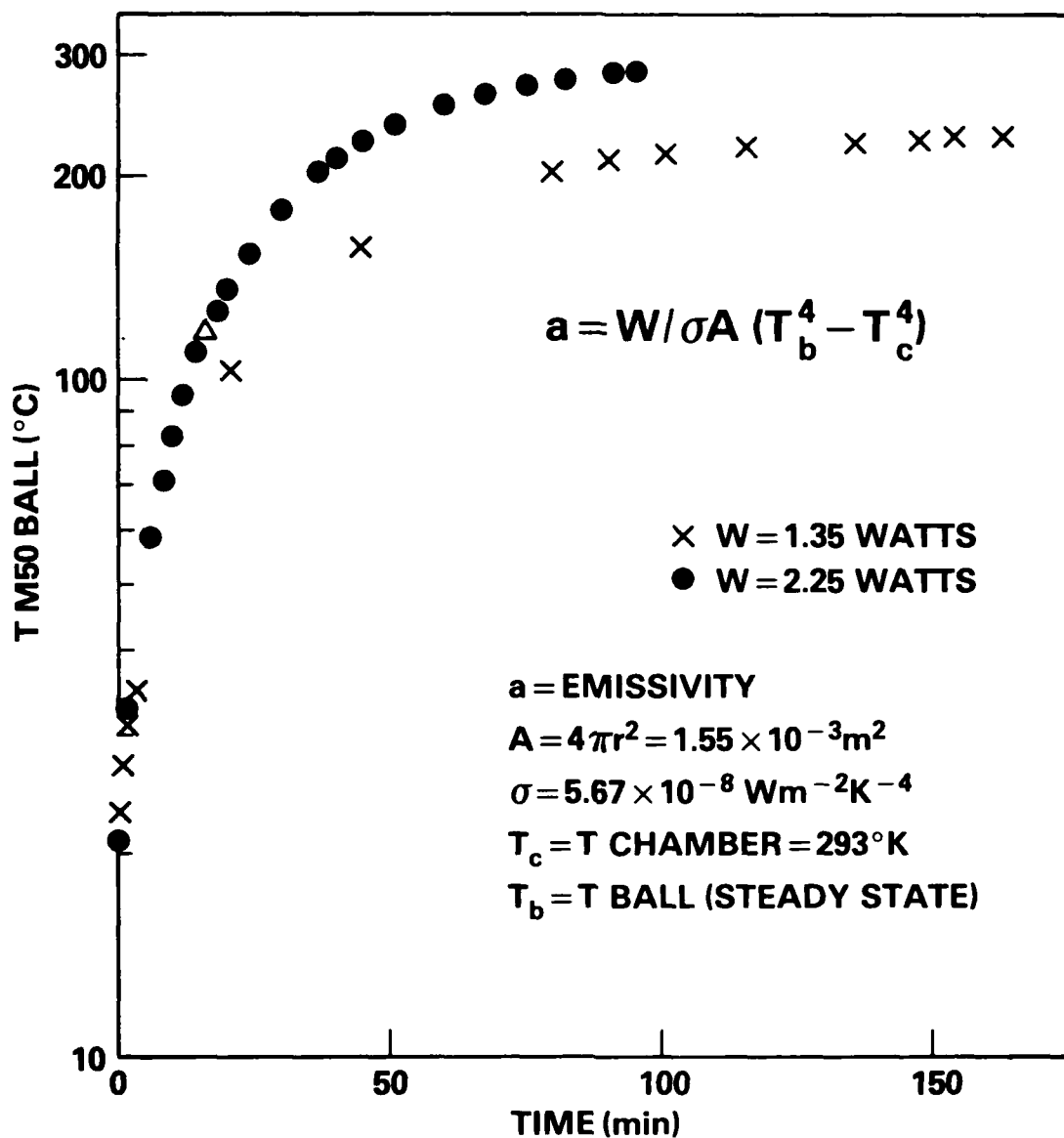
FIG. 23. The increase in temperature as a function of time of an M50 steel ball from a J-79 main shaft bearing for two different values of the ion beam input power. Form this data the emissivity of the M50 ball is determined to be 0.25.

The conditions for the performance and the endurance testing are given in Table VIII. For fatigue endurance testing the loads are much higher than would be expected in actual operation. This is done to accelerate fatigue spalling so that failures will be obtained in a reasonable period of time on a large number of bearings. For simplicity and reliability the machine rotating speed is usually kept low. Bearings in both performance tests successfully completed the scheduled 400 hour test without failure and were capable of continued operation. Fatigue test results for the fatigue endurance bearings are shown in Table IX. All bearings experienced a fatigue spall at the endurance life indicated (in hours) except where noted. The data from each group were assumed to be distributed as a Weibull function, which is a population distribution normally used to fit contact fatigue data.[9] For each group of data, Weibull distribution parameters, which are used for comparison between groups, were calculated using a least squares regression analysis. They are the L10 life, L50 life, and the Weibull slope ($\hat{\beta}$) and listed in Table IX. These are defined as follows:

    a. L10 life - The number of hours exceeded by 90% of the population,

    b. L50 life - The number of hours exceeded by 50% of the population,

    c. Weibull slope ($\hat{\beta}$) - The slope of the computed Weibull line. This parameter indicates the amount of scatter in the data.

Using the method described in reference 9, a statistical comparison was made of the L10 and L50 lives of each implanted group against the baseline unimplanted group. The results show no significance difference in fatigue lives among any of the three groups. This is evident by the large amount of overlap in the 90 percent confidence intervals around the L10 and L50 Weibull parameters as shown in Table IX.

Energy dispersive X-ray analysis were conducted to ascertain the Cr content in surface one roller before and after endurance testing. The results are shown in the X-ray spectrum of Figure 24 which includes an unimplanted roller for baseline comparison at the bottom, implanted and fatigue tested in the middle, and as-implanted at the top. It can be seen that after running for 420 hours, there is very little depletion of Cr in the roller surface. The Cr signal is positioned close to 5 keV.

V. Conclusions

Implantation of a single element (Chromium) or dual elements (Chromium plus Phosphorous or Molybedum) substantially improves resistance to both general and pitting corrosion in M50 steel. The improvements are strongly evident in three independent methods, i.e., (1) cylinder-on flat simulation (2) polarization in $IN-H_2SO_4$ and polarization in 0.1M or 0.01M NaCl solution.

Implantation jigs have been designed and built which enable the inner and outer bearing race surfaces, rollers and balls to be implanted to adequate fluences for corrosion protecion. The temperatures of the bearing components may be adequately controlled during implantation so that there is no loss of hardness (change in microstructure).

TABLE VIII

TEST CONDITIONS FOR PERFORMANCE AND FATIGUE ENDURANCE TESTING OF IMPLANTED BEARINGS

| | Performance Tests | | Fatigue Endurance Tests | | |
| | | | T58 Modified | | |
	J79 Brg.	T58 Brg.	Group 1	Group 2	Group 3
Implanted Specie(s)	Cr+Mo	Cr+Mo	Cr+P	Cr	Untreated
Load					
Radial	900 lbs.	150 lbs.	-	2800 lbs.	-
Thrust	6922 lbs.	0	-		-
Speed	7460 rpm	19,500 rpm	-	7000 rpm	-
Oil in Temp.	300°F	250°F	-	210°F	-
Oil Flow	1.45 gals/min	0.35 gals/min	-	0.25 gals/min	-
Length of Test	400 hours	400 hours	-	Until Failure	-
No. of Bearings Tested	1	1	10	10	10

Note: Lubricant - MIL-L-23699

TABLE IX

RESULTS OF FATIGUE ENDURANCE TESTS

(Hours to Failure)

	Cr+P	Cr	Untreated
	81.7	36.2	76.2
	92.6	94.4	86.9
	93.0	127.4	113.2
	100.1	132.8	177.6
	191.4	135.1	177.9
	191.7	150.9	221.9
	278.4	193.4	296.8
	351.8*	252.2	361.4*
	361.2	306.9*	383.8
	420.4*	399.3	394.3*
L_{10} Life	61.2	51.2	73.2
90% LCL	22.7	18.8	29.9
90% UCL	256.9	218.4	267.2
L_{50} Life	203.3	172.5	216.4
90% LCL	129.6	109.4	144.0
90% UCL	319.3	272.1	323.2
β	1.56	1.55	1.73

*Bearing test suspended prior to failure
LCL = Lower Confidence Limit
UCL = Upper Confidence Limit
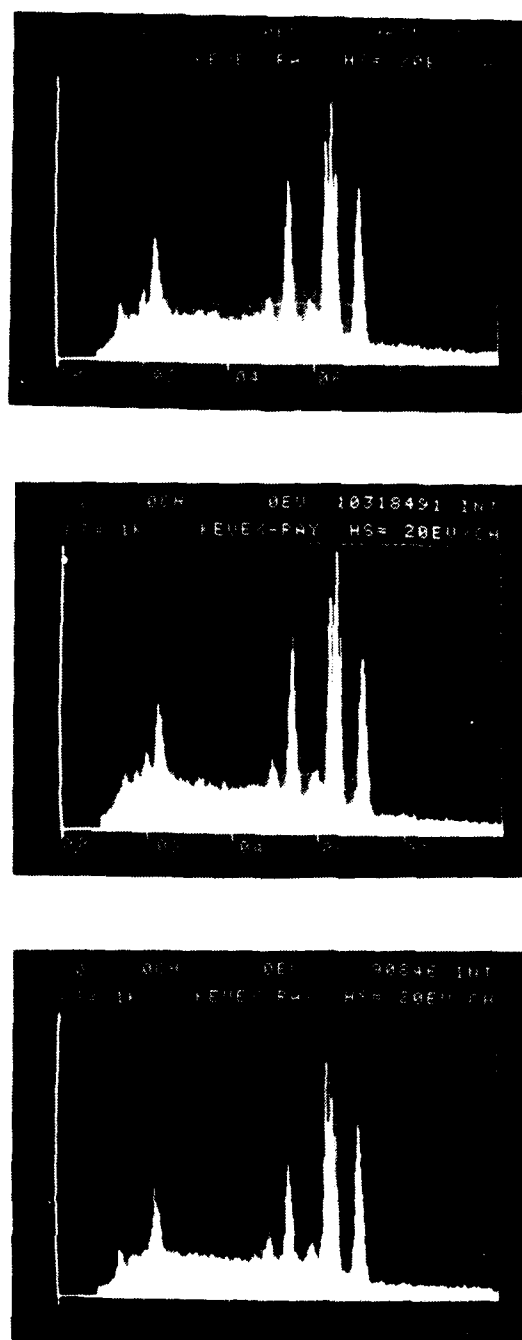
FIG. 24. Energy dispersive x-ray spectra of M50 steel rollers from a T-58 main shaft bearing. Top - Cr+P implanted but not endurance tested. Middle - Cr+P implanted and after 420 hours of endurance testing. Bottom - Not implanted and not endurance tested. The 3 spectra are normalized to the Fe K_{α} line for easy comparison. The Cr K_{α} line is considerably larger in the top and middle spectra than in the bottom spectrum.

Twenty-three T58 bearings, four T63 bearings, and one J79 bearing have been successfully implanted. The average time to implant one complete T58 bearing with Cr was 3 to 4 hours beam time. This was under less than optimum production line conditions. It is estimated that this figure could be improved by at least an order of magnitude in a production line situation.

Implantation of the ion species evaluated does not adversely affect either bearing performance and fatigue endurance life.

With currently available ion sources, such as those being used in high-throughput commercial semiconductor ion implanters, it should be possible to produce currents of up to approximately 10 mA of Cr ions. This would correspond to an implantation time of about 1.6 sec/cm^2 to reach a fluence of (10^{17} atoms/cm^2). If an operating cost of \$75/hour is assumed, this time corresponds to costs of roughly \$0.03/cm^2. Further development of dedicated ion sources should increase attainable ion currents and hence lower costs.

VI. Acknowledgments

41

Appendix

Implantation conditons for various samples.

Sample	Ion	M50 Target	Fluence $(\times 10^{17}/cm^2)$	Energy (keV)
92878L	Al	1" rod	0.6	50
	Al		0.9	100
92978L	Al	same as 92878L		
92978L	Al			
101878L	Cr	6" RCF rod	1.1	150
102678L	Cr	RCF ring	2.2	150
	Cr	new spot	1.0	150
102778L		same as 102678L		
11178L	N_2	RCF ring	1.0	150
	N_2	new spot	1.0	150
	Cr		2.0	150
	Ti	new spot	2.0	55
11878	Ti	1" rod	2.0	55
111378	Ti			
111478	Ti	same as 11878		
111478	Ti			
11978L	Cr	1" rod	2.0	150
	Mo		0.5	100
	N		0.1	12.5
	N		0.2	25
111378L	Cr	1" rod	2.0	150
	Mo		0.5	100
111478L	Cr,Mo,N	same as 11978L		
111478L	Cr	1" rod	1.1	150
	Mo		0.5	100
111578	Ti	button	2.0	55
111578	Ti			
111678	Ti	same as 11578		
111678	Ti			
112778L	Al	button	0.6	50
	Al		1.0	100
112778L	Al			
112778L	Al	same as 112778L		
112778L	Al			
1379L	Xe	J79 ball	0.3	150
1479L	Xe	J79 ball	0.3	150
1579L	Xe	J79 ball	emissivity exp.	
1879L	Xe	J79 ball	emissivity exp.	
2179	Mo	button	0.5	100
	Cr		1.5	150
	N		0.1	12.5
2179	Mo		0.5	100
2579H1	N	button	0.2	25
	N		0.32	50
	Cr		1.5	150
	Mo		0.5	100

Sample	Ion	M50 Target	Fluence $(\times 10^{17}/cm^2)$	Energy (keV)
2579H2				
2579H3	N,Cr,Mo	same as 2579H1		
2579H4				
2779H1	Cr	button	1.5	150
2779H2	Cr			
2779H3	Cr	same as 2779H1		
2779H4	Cr			
2879H1	Cr	button	1.5	150
	Mo		0.5	100
2879H2	Cr,Mo			
2879H3	Cr,Mo			
21579H1	Cr,Mo	same as 2879H1		
21579H2	Cr,Mo			
21579H3	Cr,Mo			
31579H1	Cr,Mo			
31579H2	Cr,Mo			
31579H3	Cr,Mo			
2879H4	Cr	button	1.5	150
	P		0.5	40
31579H4	Cr,P			
31579H5	Cr,P	same as 2879H4		
31579H6	Cr,P			
31679H1	Cr,P			
31579H3	Cr	button	1.5	150
	Mo		0.5	100
	N		0.1	12.5
31679H2	Cr	button	1.5	150
31679H3	Cr	button	1.5	150
31679H4	Cr	button	1.5	150
31679H5	Cr	ESCA	1.5	150
	Mo		0.5	100
31679H6	Cr,Mo	same as 31679H5		
31679H7	Cr	1" rod	1.5	150
31679H8	Cr	1" rod	1.5	150
31679H9	Cr	1" rod	1.5	150
31679H10	Cr	1" rod	1.5	150
31679H11	Cr	button	1.5	150
	Mo		0.5	100
31679H12	Cr,Mo			
31679H13	Cr,Mo	same as 31679H11		
31679H14	Cr,Mo			
31679H15	Cr	button	1.5	150
	B		2.0	40
31679H16	Cr,B	same as 31679H15		
31979H1	Mo	button	0.5	100
31979H2	Mo	button	0.5	100
31979H3	Mo	button	0.5	100
4379H1	Ti	button	2.0	55
4379H2	Ti	button	2.0	55
32979L1	Al	button	0.6	50
	Al		1.0	100

Sample	Ion	M50 Target	Fluence $(\times 10^{17}/cm^2)$	Energy (keV)
32979L2	Al	same as 32979L1		
32379H2	Ti	button	0.6	150
32379H3	Ti	button	0.6	150
42079H1	Cr	button	2.0	150
	Mo		0.35	100
42079H2	Cr,Mo	same as 47079H1		
42079H3	Cr	button	4.0	150
42079H4	Cr	button	4.0	150
6679	Cr	6" RCF rod	2.0	150
	Mo		0.35	100
61179H1	Cr	button	1.5	150
61179H2	Cr	button	1.5	150
61179H3	Cr	button	1.5	150
61179H4	Cr	button	1.5	150
82779H1	Cr	button	2.0	150
	Mo		0.35	100
82779H2	Cr,Mo			
82779H3	Cr,Mo	same as 82779H1		
82779H4	Cr,Mo			
82779H5	Cr,Mo			
82779H6	Cr,Mo			
82779H7	Cr	button	2.0	150
82779H8	Cr	button	2.0	150
82779H9	Cr	button	2.0	150
82779H10	Cr	button	2.0	150
82779H11	Cr	button	2.0	150
82779H12	Cr	button	2.0	150
82779H13	Cr	button	2.0	150
82779H14	Cr	button	2.0	150
82779H15	Cr	ESCA	2.0	150
	Mo		0.35	100
82779H16	Cr,Mo	same as 82779H15		
82779H17	Cr	ESCA	2.0	150
82779H18	Cr	ESCA	2.0	150
82879H1	Mo	button	0.35	100
82879H2	Mo	button	0.35	100
82879H3	Mo	button	0.35	100
82879H4	Mo	button	0.35	100
82879H5	Mo	button	0.35	100
12280H1	Cr	button	1.5	150
	Mo		0.5	100
12280H2	Cr,Mo	same as 12280H1		
12280H3	Cr	button	2.0	150
	Mo		0.35	100
12280H4	Cr,Mo	same as 12280H3		
13080H1	Cr	button	3.0	150
	P		1.0	40
13080H2	Cr,P			
13080H3	Cr,P	same as 13080H1		
13080H4	Cr,P			
13080H5	Cr,P			

References

1. Gary Kuhlman, Bearing Shop, NARF-NORIS, private communication.

2. Y. F. Wang, C. R. Clayton, G. K. Hubler, W. H. Lucke, and J. K. Hirvonen, Thin Solid Films, 63, 11 (1979).

3. J. K. Hirvonen, J. Vac. Sci. Technol., 15, 1662 (1978).

4. G. Dearnaley, J. H. Freeman, R. S. Nelson, and J. Stephan, Ion Implantation (North Holland, Amsterdam, 1973).

5. N. D. Tomashov, Theory of Corrosion and Protection of Metals, (the Macmillan Company, New York, 1966).

6. J. R. Ambrose, Corrosion, NACE, 34, 27 (1978).

7. J. L. Whitton, W. A. Grant, and J. S. Williams, Proc. Int. Conf. on Ion Beam Modification of Materials, Budapest, Hungary (1978).

8. J. E. Truman, M. J. Coleman, and K. R. Pirt, Br. Corros. J., 12, 236 (1977).

9. C. Brown, F. Feinberg, Development of Corrosion-Inhibited Lubricants for Gas Turbine Engines and Helicopter Transmissions, ASLE Preprint No 80-AM-6C-3 presented at 35th Annual Meeting, May 5-8, 1980.

10. C. R. Gossett, Nucl. Instrum. Methods, 168, 217 (1980).

11. J. K. Hirvonen, C. A. Carosella, and G. K. Hubler, Proceedings of Ion Implantation Equipment Conference, July, 1980, Hamilton, Ontario, Canada, to be published.

12. N. E. Anderson, Long Term Hot-Hardness Characteristics of Five Through-Hardened Bearing Steels, NASA Tech. Paper 1397, AVRADCOM Tech. Rept. 78-16, October (1978).

ATE
MED
-8